Stockholm University

π-junctions in the Kitaev chain

Master Thesis in Theoretical Physics
60 credits

Author:
Nikolaos Palaiodimopoulos

Supervisor:
Prof. Thors Hans Hansson

Co-supervisor:
Dr. Eddy Ardonne

February 7, 2016

Abstract

The Kitaev chain model, that describes an one-dimensional spinless p-wave superconductor which can support topological protected states at its boundaries, was introduced fifteen years ago. Since then a lot of effort has been made to realize this model experimentally and probe these states mainly through transport experiments. In this work we review the topological phases that can arise in the model by considering setups in which, by varying the superconducting order parameter from a positive to a negative value we effectively create a π-junction. Depending on whether the order parameter is real or complex one can form a real or a phase-winding π junction. By taking advantage of the properties of these junctions we explain and numerically simulate how the zero modes that sit at the edge of the chain interact with each other when three chains are brought close together. Finally using the Landauer-Büttiker formalism we numerically investigate the transport properties of the Kitaev chain for different profiles of the superconducting order parameter. We conclude that the localization of a fermionic mode (consisting of two Majorana modes) at the center of the junction, leads to the appearance of a zero bias peak in the transmission spectrum of an electron tunneling through the chain and we make some speculations concerning the nature of this peak.

Acknowledgments

I would like to express my graditude to my supervisor Thors Hans Hansson and my co-supervisor Eddy Ardonne for their support and guidance throughout this project, it was my pleasure learning and working with them. Secondly, I am very thankful to Christian Spånslätt for taking the time to work with me, helping me with the coding and having the patience to anwser all my "stupid" questions. Furthermore, I would like to thank all my friends and teachers at Stockholm University who made it possible for me to enjoy to the fullest the last two years of my studies. Last but not least, I am grateful to my family for their help and support and to Panagiota for always being there for me.

Contents

Chapter 1

Introduction

The Dirac equation, that describes spin-1/2 particles, can be written down, in covariant form as follows:

$$(i\gamma^\mu \partial_\mu - m)\psi = 0 \tag{1.1}$$

At 1937 Ettore Majorana, before mysteriously dissapearing off the face of the earth, in his famous paper [21] discovered a purely imaginary representation of the gamma matrices that led him to the conclusion that the Dirac equation can have real solutions. The fact that ψ can be real meant that fermionic particles, which are there own anti-particles, could exist and they were called Majorana fermions.

In high energy physics up until now no fundamental particle has been identified as a Majorana fermion. Neutrinos are considered as a possible candidate and experiments are trying to observe a process that is called neutrinoless double beta decay [17], this process violates the lepton number conservation and it would provide a strong indication that neutrinos are Majorana fermions. Moreover other candidates come from supersymmetry were theory suggests that some superpartners mirror the properties of their partners and they are their own antiparticles [34].

In condensed matter physics the basic ingredients of the systems we are considering are electrons and ions so in this case the Majorana "particles" correspond to excitations that emerge from the collective behavior of these building blocks. These excitations consisting of the fundamental particles of the system "dressed" with the interactions are called quasiparticles, when we can employ a free Hamiltonian in order to describe their behavior and assign them physical properties such as an effective mass, charge etc.. The concept of emergence is fundamental in condensed matter physics since in most of the cases, even though we know the basic laws that govern the behavior of the fundamental constituents, an analytic solution cannot be obtained by any means. Nevertheless from all the "mess" beauty arises at different scales and by employing effective theories the necessary models for describing emergent excitations can be constructed. By effective theories we mean theories that have a cut off (usually a particular energy scale) beyond which the theory is no longer valid.

Concepts of topology were linked to condensed matter theory at first with the study of topological defects [14] and later on with the discovery of what are now called topologically ordered states [32]. These states belong to the broader category of quantum ordered states. One of the main characteristics of these states is the fact that they cannot be explained by Landau's theory of symmetry breaking. The main reason for this is that at zero temperature the quantum effects cannot be ignored and no local ordered parameter can be employed to describe the properties of the ground state. The discovery of the integer and especially of the fractional quantum Hall effect (FQHE) [30] drew the community's attention to these states of matter and since then a lot of research has been done in order to understand them. Some of the most interesting properties of the FQHE like fractional charge, fractional statistics and chiral edge states have their roots in topology.

Systems that support topological phases often have topologically protected states that "live" on their boundaries. The realization of the Majorana particles in condsensed matter physics are such edge states and because these states lie at zero energy they are called zero energy modes. The physical platform where these modes are realized are topological superconductors

or many-body systems that effectively behave like superconductors [10]. Famous examples of theoretical models where the Majorana modes emerge are the Moore-Read states of the FQHE [25], the two-dimensional $p + ip$ spinless superconductor [18] and the one-dimensional p-wave spinless superconductor [15].

In the last few years many experimental groups have tried to verify the existence of the Majorana modes in condensed matter systems. Most of them tried to realize the 1D spinless p-wave superconductor in different setups and probe the existence of the zero modes through tunneling experiments. Although there are experimental results that strongly support the existence of these modes [22],[23], there is no conclusive evidence yet, since there are still some effects like, for example, disorder [20] that is alleged to be able to produce the same experimental signatures.

The most important potential application of these modes, which makes it so appealing to be able to create and control them, is quantum computation. As we mentioned these Majorana modes do not correspond to the physical degrees of freedom and as we will see later on, for the one-dimensional p-wave spinless superconductor, one needs to combine two such modes to obtain a single fermionic degree of freedom, which means that the fermion number is fractionalized. So, having two Majorana modes spatially separated, one effectively creates a delocalized fermionic mode that can be used as a qubit which will automatically be robust to decoherence due to its non-local nature.

In this thesis we will focus on the one-dimensional spinless p-wave superconductor which is often called the Kitaev chain and can support two Majorana modes at its ends. By varying the superconducting order parameter in this system from a positive to a negative value, we can effectively form a π-junction. Depending on how the variation occurs a different number of Majorana zero modes appears in the junction. So by exploiting the properties of these junctions we will examine the case where the ends of three Kitaev chains are brought close to each other and more specifically focus on the interaction between the three Majorana modes. Moreover we will explore the transport properties of the Kitaev chain when such π-junctions are formed along the chain.

1.1 Outline

Chapter 2: In this chapter we are reviewing the one-dimensional model that was introduced by Kitaev [15]. To be able to understand better, under which conditions the Majorana zero modes emerge in this model, we numerically implement the Kitaev Hamiltonian in $Mathematica^{®}$ and by exact diagonalization in real space we obtain the eigenvalues and eigenvectors of the model. Finally we briefly review one of the most important schemes that has been proposed in order to effectively create an equivalent Hamiltonian in an experimental setup.

Chapter 3: Here concepts of topology are linked with the bulk spectrum of the free fermionic Hamiltonians. We present the topological clasiffication that has been proposed in order to clasify the Hamiltonians based on the three fundamental discrete symmetries. Also we identify which are the symmetry classes that correspond to the Kitaev Hamiltonian and we sketch how one can construct the topological invariant for each case.

Chapter 4: Based on the properties of the real π and of the phase-winding junction that have been studied in [29] we investigate how three Majorana zero modes interact with each other when the ends of three topological wires are brought close together forming a tri-junction. We highlight the importance of the p-wave nature of the superconducting order parameter that induces a particular direction in the superconducting coupling and furthermore we numerically simulate our setup in order to verify our results.

Chapter 5: We quickly review the Green's function formalism that is used to study the transport properties of normal mesoscopic systems and afterwards the formalism is generalized in order to be able to describe superconducting systems. By employing the above formalism we obtain the relations that give the local density of states and the transmission probability of an electron tunneling into the wire. Afterwards by using the Landauer-Büttiker formalism we derive the con-

ductance for a normal-superconducting (NS) interface and for a normal-superconducting-normal (NSN) setup. Our approach follows closely Datta's book: *Electronic transport in mesoscopic systems* [7] while the generalization to the superconducting systems and the derivation of the conductance is based on the paper: *Scattering theory of transport for mesoscopic superconductors* [9].

Chapter 6: We use the transport theory that was reviewed in the previous chapter in order to numerically simulate different setups and see how the presence of the Majorana modes affects the conductance spectrum. At first we simulate the NS interface and reproduce the zero bias peak that has been observed experimentally and is alleged to be a characteristic signature of a Majorana zero mode that sits on the interface. Then we present our numerical results concerning the conductance of a NSN setup for three different profiles of the superconducting order parameter, namely for a constant order parameter, for a real π-junction and for a phase winding junction.

Chapter 7: In this chapter, a brief summary of what has been done in this work is followed by a discussion concerning the interpretation of our numerical results. We highlight the conclusions that can be drawn from this study, the questions that remained open and propose directions for future research.

Chapter 2

A topological wire

2.1 Kitaev's chain

At 2001 Kitaev introduced his famous toy model [15] for an one-dimensional, spinless p-wave superconductor. The beauty of this model lies on its simplicity; it is the simplest model that can support Majorana zero modes. In this chapter we will review the basic properties of this model. We will assume that the reader is familiar with the second quantization formalism, if not an excellent introduction on the subject can be found in [3]. We will start by writing the Kitaev's one-dimensional tight-binding Hamiltonian in real space [1]:

$$\mathcal{H} = -\mu \sum_n c_n^\dagger c_n - \frac{t}{2} \sum_n (c_n^\dagger c_{n+1} + c_{n+1}^\dagger c_n) - \sum_n \frac{|\Delta|}{2} (e^{i\phi} c_n c_{n+1} + e^{-i\phi} c_{n+1}^\dagger c_n^\dagger) \tag{2.1}$$

where n labels the sites, μ is the chemical potential, t is the hopping amplitude and Δ, ϕ the superconducting pairing amplitude and phase respectively. Also, the c_n's correspond to the fermionic operators that annihilate an electron at site n and $c_n^\dagger$'s to the creation and they obey the fermionic anti-commutation relations $[c_i, c_j^\dagger]_+ = \delta_{ij}$ and $[c_i, c_j]_+ = [c_i^\dagger, c_j^\dagger]_+ = 0$. We now draw the reader's attention to the last term that describes the superconducting coupling between the electrons. Note here that the electrons of this model have one spin component, which makes them effectively spinless, so we have an unconventional superconducting pairing that differs from the usual s-wave pairing, where the Cooper pairs are formed by electrons with opposite spin. Also, due to Pauli's principle, the superconducting coupling applies to electrons from adjacent sites.

Now let us consider the above Hamiltonian with open boundary conditions, the fermionic operators c_n can be decomposed into two Majorana operators that can be defined in the following way:

$$\gamma_{2n-1} = c_n + c_n^\dagger, \quad \gamma_{2n} = \frac{c_n - c_n^\dagger}{i}, \quad n = 1, ..., N \tag{2.2}$$

using the fermionic anti-commutation relations we can see that these operators obey the anti-commutation relation $[\gamma_i, \gamma_j]_+ = 2\delta_{ij}$ and aslo satisfy the relation $\gamma_m^\dagger = \gamma_m$. This is just a change of basis and of course we are not literally saying that the electron consists of two Majorana particles, however as we will see in a while, it is instructive to think in this way in order to understand how the zero modes emerge in this model. Moreover it makes no sense to think γ as a particle and this becomes clear if we try to form a Majorana number operator $n_i = \gamma_i^\dagger \gamma_i$ which based on the properties of the γ operators is always equal to 1. The only states that can be emty or occupied are the fermionic states and the "correct" number operator is given by $n_i = c_i^\dagger c_i$. Thus we can say that γ is a fractionalized mode, since each fermionic degree of freedom consists of two Majoranas.

Inverting the above transformation and for convenience adding the superconducting phase into the definition we get:

$$c_n = \frac{ie^{-i\frac{\phi}{2}}\gamma_{2n-1} - e^{-i\frac{\phi}{2}}\gamma_{2n}}{2i}, \quad c_n^\dagger = \frac{e^{i\frac{\phi}{2}}\gamma_{2n} + ie^{i\frac{\phi}{2}}\gamma_{2n-1}}{2i} \tag{2.3}$$

and using this we can re-write our Hamiltonian in terms of the Majorana operators as:

$$\mathcal{H} = -\frac{\mu}{2}\sum_n (i\gamma_{2n-1}\gamma_{2n} + 1) + \frac{i}{4}\sum_n (t+\Delta)\gamma_{2n}\gamma_{2n+1} - \frac{i}{4}\sum_n (t-\Delta)\gamma_{2n-1}\gamma_{2n+2} \tag{2.4}$$

Following Kitaev's argument we will focus on two special cases, namely:
(i) When $\mu < 0$ and $t = \Delta = 0$, the Hamiltonian is:

$$\mathcal{H} = -\frac{\mu}{2}\sum_{n=1}^{N} (i\gamma_{2n-1}\gamma_{2n} + 1) = -\mu\sum_n c_n^\dagger c_n \tag{2.5}$$

Here the spectrum is gapped and the ground state is not degenerate and corresponds to the fermionic vacuum.
(ii) When $\mu = 0$ and $t = \Delta \neq 0$, we have:

$$\mathcal{H} = \frac{it}{2}\sum_{n=1}^{N-1} \gamma_{2n}\gamma_{2n+1} \tag{2.6}$$

In this case we can see that the operators do not belong to the same site of the chain and pairs are formed from adjacent sites. Also note that the operators γ_1 and γ_{2N} are absent from the Hamiltonian, so we end up with two zero energy modes that are localized in the two ends of our chain. Using these two modes we can construct a non-local fermionic operator:

$$\tilde{c} = \frac{1}{2}(\gamma_1 + i\gamma_{2N}) \tag{2.7}$$

The ground state now has a two-fold degeneracy corresponding to this mode being occupied or empty. One can define the parity of a ground state as the eigenvalue of the number operator of the above non-local fermionic operator and the two ground states have even or odd parity. The different pairing corresponding to the two cases that were mentioned above is nicely depicted in figure 2.1. Now also it is clear why the electrons of the original Hamiltonian had to be spinless. If the spin degree of freedom was present we would have two Majorana modes at each end that they would gap out forming a normal fermion with finite energy.

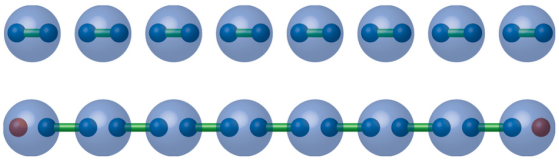

Figure 2.1: The first chain illustrates the trivial case where the Majoranas from the same site are paired together and the edge modes are absent. The chain below shows the non-trivial case and the red spheres at the two ends of the chain represent the Majorana modes, picture taken from [11].

2.2 Numerical implementation

The Kitaev's Hamiltonian 2.1 can be written in a matrix form. To do that let's first define the $2N$ component vector:

$$\mathcal{C} = \begin{pmatrix} c_1 & ... & c_N & c_1^\dagger & ... & c_N^\dagger \end{pmatrix}^T \tag{2.8}$$

where N is the number of sites of the chain. By this we have doubled our degrees of freedom and we can think that the c operators correspond to particles while the $c^\dagger$ to holes. Note however, that one cannot think these particles and holes to be the physical excitations of our system like in the case of a semiconductor. Our physical degrees of freedom remain N and the excitations of the system are superpositions of particles and holes. This will become clearer mathematically when we derive analytically the spectrum of the bulk Hamiltonian.

The doubled Hamiltonian becomes:

$$\mathcal{H} = \mathcal{C}^\dagger H \mathcal{C} \tag{2.9}$$

to illustrate how this matrix looks like, we consider an example of a three-site chain, where the matrix H takes the following form (omitting some factors of 2):

$$\begin{pmatrix} -\mu & -t & 0 & 0 & \Delta e^{-i\phi} & 0 \\ -t & -\mu & -t & -\Delta e^{-i\phi} & 0 & \Delta e^{-i\phi} \\ 0 & -t & -\mu & 0 & -\Delta e^{-i\phi} & 0 \\ 0 & -\Delta e^{i\phi} & 0 & \mu & t & 0 \\ \Delta e^{i\phi} & 0 & -\Delta e^{i\phi} & t & \mu & t \\ 0 & \Delta e^{i\phi} & 0 & 0 & t & \mu \end{pmatrix} \tag{2.10}$$

In general this is a $2N \times 2N$ matrix and based on our previous interpretation of the elements of the $\mathcal{C}$ vector, the upper left $N \times N$ block of this matrix corresponds to particles, the down right to holes and the off diagonal blocks to the superconducting coupling. We can now put this matrix in Mathematica® and diagonalize it by "brute force" (exact diagonalization) to obtain the eigenvalues and eigenvectors of the real space Hamiltonian.

Considering a chain of $N = 40$ sites and restraining ourselves to the case where the superconducting order parameter is real ($\phi = 0$), we simulate cases (i) and (ii) and in figure 2.2 we plot the eigenvalues of the Hamiltonian matrix for the two cases.

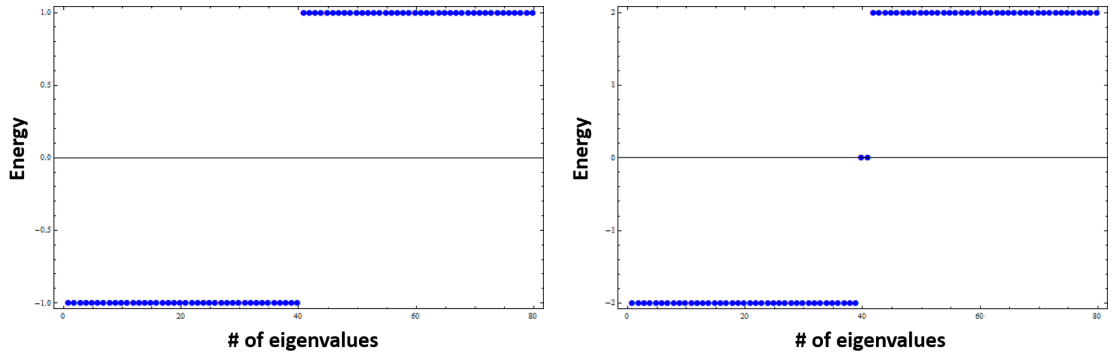

Figure 2.2: Left: eigenvalues for the trivial case, gapped spectrum with no zero modes present ($\mu = 1.0$, $t = \Delta = 0$). Right: non-trivial casel, gapped spectrum with two modes at zero energy ($\mu = 0$, $t = \Delta = 2.0$).

Note here that the spectrum is symmetric above and below zero energy this is the particle-hole symmetry that we introduced to our system when we doubled the degrees of freedom.

Let us focus on the non-trivial case and see how the zero modes behave when we are changing the values of the parameters. First of all, if we let Δ differ from the hopping parameter t then the spectrum takes the standard cosine form. Thus we end up with two cosine bands of positive and negative energy separated by the gap and the zero modes are still present. The interesting thing however occurs when we keep the values of Δ and t fixed and we let μ increase, then the zero modes persist as long as $\mu < t$. Also due to symmetry the same thing happens if we let μ decrease until $\mu > -t$. So we conclude that the zero modes appear in this model as long as $|\mu| < t$. What makes the value $\mu = t$ ($\mu = -t$) so special is that at this point the gap closes and if we keep increasing (decreasing) μ beyond this point the gap re-opens but the zero modes are gone (figure 2.3).

Finally we want to illustrate how the modes are localized at the two ends of the chain. In order to do that we extract the eigenvectors that correspond to the two zero eigenvalues. Using these eigenvectors and keeping their particle part (just the first N elements), since the hole part is the same due to symmetry, we can plot the wave function amplitude of the modes. As Kitaev predicted in his paper, the two modes are exponentially localized at the ends of the chain, this is clearly illustrated in the logarithmic plot. The two modes are localized at the edges in the

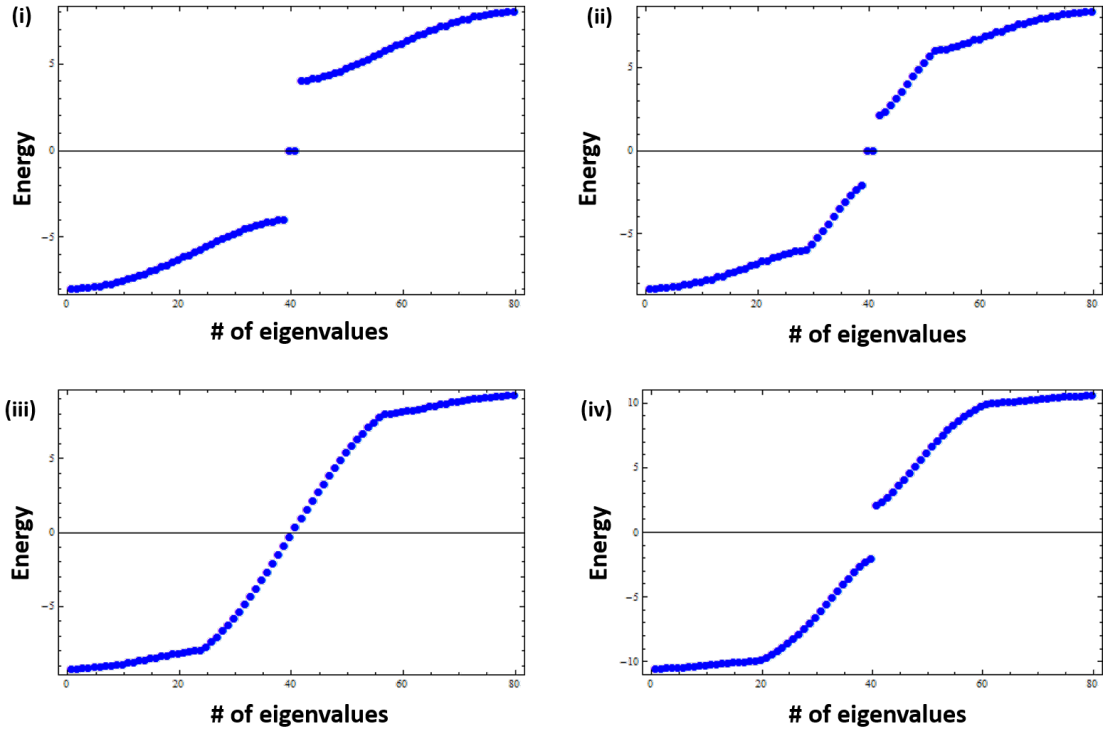

Figure 2.3: How the spectrum varies as we increase μ ($N = 40$, $t = 2.0$ and $\Delta = 4.0$). (i) $\mu = 0$, (ii) $\mu = 2.0$, (iii) $\mu = 4.0$, (iv) $\mu = 6.0$.

limit $N \to \infty$. If the chain is finite there is a small interaction between the two modes that is proportional to $e^{-N/\xi}$, where ξ the superconducting coherence length of the system. This interaction results in an exponentially small energy splitting and the fermion mode acquires a finite energy but as long as $\frac{N}{\xi} \gg 1$ we can consider it negligible.

To conclude, when we first introduced the non-trivial case one would think that the appearance of the zero modes in this model is a consequence of the fine-tuned parameters and if we would move away from these particular values the zero modes would disappear. However we saw that this is not the case and in the following chapter we will elaborate the reasons why by exploiting the bulk's topology.

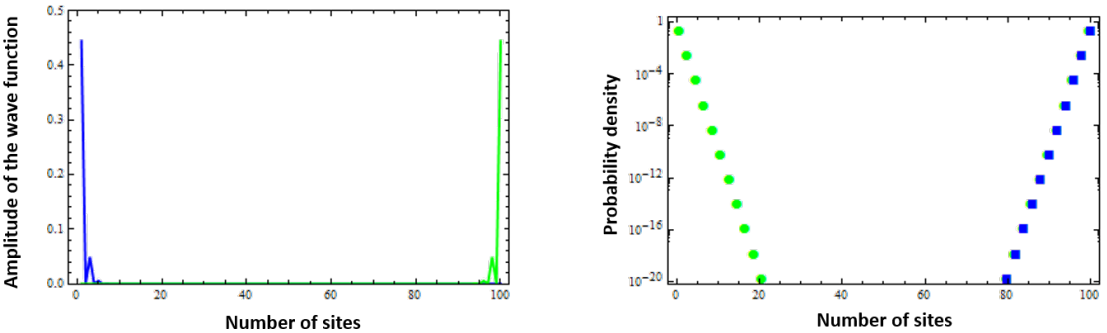

Figure 2.4: Left: Wave function amplitude for the two zero modes. Right: Logarithmic plot of the amplitude squared.

2.3 A more realistic Hamiltonian

As we mentioned before, the toy model that we have introduced in the previous sections is very appealling due to its simplicity, so a lot of effort has been made to create a realistic setup that can be effectively described by Kitaev's Hamiltonian. Spinless electrons is not something you can find in nature and as for p-wave superconductivity, eventhough there are some materials that are believed that they support p-wave pairing [13], up to now there is no sufficient evidence to verify this claim. More than one schemes has been proposed to realize this model, here we will review the one that has been proposed in [27, 24] and has been applied to various experimental setups.

Three are the necessary ingredients that one needs in order to construct the effective Hamiltonian; spin-orbit coupling, an s-wave superconductor and magnetic field. We will scetch how the combination of these three ingredients leads to the desired result, without going into much details, based on the excellent review paper of Alicea [1]. The Hamiltonian in this case is given by:

$$\mathcal{H} = \int dx\, \psi^\dagger \Big(\frac{\partial_x^2}{2m} - \mu - i\alpha\sigma^y\partial_x + h\sigma^z \Big)\psi + \Delta(\psi_\uparrow\psi_\downarrow + h.c) \tag{2.11}$$

In the Hamiltonian above the third term inside the parenthesis describes the spin-orbit interaction, the fourth term correspond to the magnetic field and the last term to the conventional s-wave pairing.

In the experimental setups a one dimensional nanowire with strong spin orbit coupling (InAs or InSb) is placed next to an s-wave supeconductor, thus the superconductivity is induced to the wire by the proximity effect. The right picture of figure 2.5 illustrates the band structure of the nanowire. Without the spin-orbit term and the Zeeman term, the dispersion relation would have the usual parabolic shape, when the spin-orbit term is added the spin degeneracy is lifted and two shifted parabolas are formed corresponding to spin up and spin down (dotted blue lines). There is one crossing between these two parabolas at $k = 0$, but when the magnetic field is turned on the crossing dissapears and two seperated energy bands are formed due to the Zeeman splitting (black solid lines).

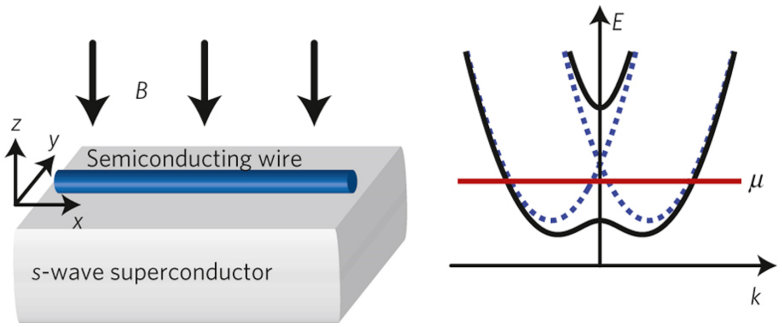

Figure 2.5: Left: Nanowire placed on top of the s-wave superconductor. Right: Band structure of the wire, picture taken from [2].

Thus when the chemical potential lies in the region between the two bands the wire can be considered as "spinless" and by inducing superconductivity we effectively create the p-wave pairing. Two crucial things for this approach to work are, first that the spin-obit interaction should be perpendicular to the magnetic field and secondly the superconducting order parameter must be small compared to the magnetic field $\Delta \ll h$.

Chapter 3

How topology comes into play

The field of topology is concerned with the properties of space that remain intact when we apply continuous deformations. In quantum mechanics the adiabatic theorem roughly states that if we start with a system being in one of its eigenstates whose eigenvalue is separated from the other states by a finite energy gap, then it will remain there as long as the Hamiltonian will evolve sufficiently slow compared to the energy of the gap. So by making the connection between these two concepts we can say that two systems are in the same topological phase if their Hamiltonians can be transformed into each other without closing the energy gap. The topological band theory in condensed matter studies the topological phases of systems that can be described by the band theory of solids. The band theory concerns states that can be described by single particle Hamiltonians and it is assumed that interactions can be adiabatically switched-off. Of course this assumption seems difficult to motivate for the case of superconductors where the electrons are strongly correlated, nevertheless in a mean field treatment this can be done. In order to classify systems based on their topology we have to construct a quantity that remains invariant when our Hamiltonian is in a particular topological phase and only changes when we go from one phase to another. Such a quantity is called a topological invariant and its change signifies what is called a topological phase transition. The construction of this invariant is not a trivial thing and one can define it in different ways even for the same model.

We will come back to the classification of the free fermionic Hamiltonians, but before doing that let us see how one can define a topological invariant quantity for the Kitaev chain. In order to do so, we shall first extract the bulk spectrum of the model.

3.1 Bulk spectrum

By studying the properties of the bulk we can see under which conditions the non-trivial phase of the previous chapter, that supports zero modes at the edges, arises. If we impose periodic boundary conditions to the tight binding Hamiltonian 2.1 due to the translation invariance we can go to momentum space by Fourier transforming our operators:

$$c_n = \frac{1}{\sqrt{N}} \sum_k e^{ink} c_k, \quad c_n^\dagger = \frac{1}{\sqrt{N}} \sum_k e^{-ink} c_k^\dagger \tag{3.1}$$

Furthermore by introducing the two component Nambu operator $C_k^\dagger = [c_k^\dagger, c_{-k}]$, thus doubling our degrees of freedom, the Hamiltonian can be written in the Bogoliubov-de Gennes form:

$$\mathcal{H} = \frac{1}{2} \sum_{k \in BZ} C_k^\dagger \mathcal{H}_{BdG} C_k$$

$$\mathcal{H} = \frac{1}{2} \sum_{k \in BZ} \begin{pmatrix} c_k^\dagger & c_{-k} \end{pmatrix} \begin{pmatrix} -t\cos k - \mu & i\Delta e^{-i\phi} \sin k \\ -i\Delta e^{i\phi} \sin k & t\cos k + \mu \end{pmatrix} \begin{pmatrix} c_k \\ c_{-k}^\dagger \end{pmatrix} \tag{3.2}$$

Since we are dealing with a quadratic Hamiltonian with anomalous terms, in order to obtain the diagonal form we will use the Bogoliubov transformation:

$$\alpha_k = u_k c_k + v_k c_{-k}^\dagger \tag{3.3}$$

If we express the Hamiltonian in terms of the quasiparticle operators we obtain:

$$\mathcal{H} = \sum_{k \in BZ} E(k) \alpha_k^\dagger \alpha_k \tag{3.4}$$

where the bulk energy spectrum is given by:

$$E(k) = \sqrt{(-tcosk - \mu)^2 + |-i\Delta e^{i\phi} sink|^2} \tag{3.5}$$

and k spans the Brillouin zone. Note that $\mathcal{H}_{BdG}$ can be written in terms of the Pauli matrices σ_i as:

$$\mathcal{H}_{BdG} = (-t \cos k - \mu)\sigma_z - (\Delta \sin k)\sigma_y \tag{3.6}$$

where we have taken the superconducting phase equal to zero ($\phi = 0$).

3.2 A topological invariant

Let us go back to the open chain that was introduced in the first chapter and sketch how Kitaev [15] constructs the topological invariant for this case. As you remember we saw that the two phases differ in terms of their ground states, in the trivial phase we have a unique ground state while in the topological phase the ground state has a two-fold degeneracy. In the topological phase when the delocalized fermion mode occupies the ground state its parity is odd while when it does not the parity is even. So it seems logical to try to connect our topological invariant with the parity of the ground state.

The Kitaev Hamiltonian, for general values of μ, t and Δ, can be written as:

$$\mathcal{H} = \frac{i}{2} \sum \gamma_m A_{mn} \gamma_n \tag{3.7}$$

where A_{mn} is a real anti-symmetric matrix, meaning that it is a square matrix whose transpose is also its negative. Every real anti-symmetric matrix can be brought to a block diagonal form by applying a special orthogonal transformation, each block then has the following form:

$$\begin{pmatrix} 0 & \epsilon_l \\ -\epsilon_l & 0 \end{pmatrix} \tag{3.8}$$

where $\epsilon_l \in \mathbb{R}$ the excitation energies of each fermion. For an anti-symmetric matrix the determinant can be written as the square of a polynomial in the matrix entries, $pf(A)^2 = det(A)$. This polynomial is called the Pfaffian of the matrix and can be written as a product of the eigenvalues $\prod_l \epsilon_l$. The sign of this quantity is sensitive to a zero energy crossing, in contrast to the sign of the determinant, which remains the same. Note that because of the doubling of the physical degrees of freedom the eigenvalues come in pairs that do not correspond to two distinct states but to a single Bogoliubov quasiparticle. Thus when a pair crosses zero energy the energy of the quasiparticle changes sign and likewise the fermion parity of the ground state changes from even to odd or the other way around.

Now by looking carefully the energy spectrum of the bulk we will identify the points in k-space where the topological transition takes place. So in equation 3.5, we notice that the gap closings occur when $\mu = \pm t$ for $k = 0$ and $k = \pi$. Consequently in this model we can compute the Pfaffians of $\mathcal{H}(k = 0)$ and $\mathcal{H}(k = \pi)$ (since that in all the other points nothing interesting happens) and by considering the sign of their product we end up with a quantity that stays invariant as long as the gap exists. This is our topological invariant!

$$\mathcal{M} = sgn(Pf(A)_{k=0} Pf(A)_{k=\pi}) \tag{3.9}$$

If we compute the two Pfaffians we get $Pf(A)_{k=0} = \mu - t$ and $Pf(A)_{k=\pi} = \mu + t$, which is in total agreement with the results we had obtained from the numerical simulations at chapter 2. When $\mathcal{M} = +1$ the chain is in the trivial phase on the other hand when $\mathcal{M} = -1$ the Majorana modes are present and the chain is in the topological phase. Notice also that at the transition points (gap closings) the topological invariant is ill-defined. In general the non-trivial topology of the bulk leads to the manifestation of gapless edge modes in the open system, this is the essence of what is called bulk-boundary correspondence[33].

3.3 Topological classification

At the beginning of the chapter we emphasized that it is crucial to have an energy gap in order to be able to classify the topologically equivalent states of matter but as we pointed out there is more to it than that. Namely, there is an additional requirement that has to do with the three fundamental discrete symmetries, i.e. time reversal symmetry (TRS), particle-hole symmetry (PHS) and chiral or sub-lattice symmetry (CS). Thus taking into account the presence or absence of these symmetries we can state that two Hamiltonians are topologically equivalent if they can be "continuously deformed" into one another without closing the gap and without breaking (or introducing) any of the above symmetries. Breaking a symmetry or closing the gap can lead to a topological phase transition. A classification of topological insulators and superconductors based on their symmetry classes is given in [28] and [16]. In this thesis we will restrict ourselves to the part of the classification that concerns the one dimensional topological systems in order to see which are the symmetry classes that correspond to the Kitaev chain (Table 3.1).

Table 3.1: Topological classification for one dimension

Classes	TRS	PHS	CS	$d = 1$
A	0	0	0	-
AI	+1	0	0	-
AII	-1	0	0	-
AIII	0	0	1	$\mathbb{Z}$
BDI	+1	+1	1	$\mathbb{Z}$
CII	-1	-1	1	$2\mathbb{Z}$
D	0	+1	0	$\mathbb{Z}_2$
C	0	-1	0	-
DIII	-1	+1	1	$\mathbb{Z}_2$
CI	+1	-1	1	-

The names of the symmetry classes origin from the classification of Riemannian symmetric spaces that where studied by the French mathematician Elie Joseph Cartan. The last column of this table describes the nature of the topological invariant for each case, $\mathbb{Z}$ means that the invariant takes integer values $0, \pm 1, \pm 2, ...$, $\mathbb{Z}_2$ that its value is restricted to only two integers (usually ± 1 or 0 and 1) and $2\mathbb{Z}$ that the integer values are even .

This classification was originally introduced in the context of random matrix theory in disordered systems [4]. In quantum mechanics, according to Wigner's theorem [31], symmetries can be represented by linear and unitary or anti-linear and anti-unitary operators that commute or anti-commute with the Hamiltonian. If a unitary symmetry is present the Hamiltonian matrix can be written in block diagonal form, where each block is related to an eigenvalue of the symmetry operator. Thus a unitary symmetry can be used to reduce the Hilbert space, since each block does not possess the symmetry anymore. The anti-unitary operators do not have this effect on the Hamiltonian matrix but they have an effect on the properties of the spectrum and wavefunctions [12] and this is what makes them important in our case. In the context of random matrix theory anti-unitary symmetries can be used to further analyze each block of the already partially diagonalized Hamiltonian matrix.

The two anti-unitary symmetries that appear in the above classification are time reversal ($\mathcal{T}$) and particle-hole symmetry ($\mathcal{P}$). A Hamiltonian that remains invariant under the reversion of the time arrow commutes with the time reversal operator, $[H, \mathcal{T}] = 0$. While a Hamiltonian that

is particle-hole symmetric anti-commutes with the PHS operator, $[H, \mathcal{P}]_+ = 0$. In addition to these two anti-unitary symmetries a third unitary symmetry has to be taken into account, this symmetry is called Chiral ($\mathcal{C}$) and is given by the product of the two anti-unitary symmetries $\mathcal{C} = \mathcal{T} \circ \mathcal{P}$. Chiral symmetry is a unitary symmetry which anti-commutes with the Hamiltonian $[H, \mathcal{C}]_+ = 0$.

For each of the two anti-unitary symmetries there are three possibilities, the first one corresponds to the case where the symmetry is absent, the second to the case where the symmetry is present and the symmetry operator squares to $+1$ and the third one to the case where the symmetry is present but the symmetry operator squares to -1. Considering the above possibilities for TRS and PHS we get nine symmetry classes. As for the chiral symmetry, it is always present when both TRS and PHS are present but in the case where both of them are absent CS may or may not be present. Thus by taking into account all the above we can understand why there are in total ten symmetry classes. In table 3.1 you can see which symmetries are fulfilled in each symmetry class. The zero entries mean that the symmetry is absent, while the plus or minus sign, in the case where one symmetry is present, implies that the symmetry operator squares to $+1$ or -1 respectively.

3.4 Symmetry classes of the Kitaev chain

Now lets see which symmetry classes correspond to the Kitaev Hamiltonian. First of all note, that in this case particle hole symmetry is more like a spectral constraint that was imposed when we doubled the degrees of freedom, than a physical symmetry of the system [29]. This leads to the existence of PHS that squares to $\mathcal{P}^2 = +1$. Concerning the TRS symmetry there are two scenarios, in the general case where the hopping parameter t and the superconducting coupling Δ are both complex then time reversal symmetry is broken and the system belongs to class D. On the other hand, if t and Δ are real then the system has TRS that squares to $+1$ and so the system belongs to the symmetry class BDI.

As you can see from the classification table, class D has a $\mathcal{Z}_2$ topological invariant, this is the Pfaffian invariant that was introduced in the previous section and takes the values ± 1. As for the BDI class, the invariant in this case takes integer values that correspond to a winding number. More specifically for a model with a constant superconducting order parameter we have besides the trivial one, two topological phases that correspond to $\Delta > 0$ and $\Delta < 0$, thus the topological invariant can take the values $\mathbb{Z} = -1, 0, +1$. Of course the fact that the topological invariant can only take these three values, strictly depends on the number of parameters that were included in the Hamiltonian.

To understand better the nature of the winding invariant we give an intuitive geometric interpretation of the three topological phases that arise in the BDI class [29]. Using equation 3.6 the Hamiltonian can be written as:

$$\mathcal{H} = \boldsymbol{d}(k) \cdot \boldsymbol{\tau} \tag{3.10}$$

where $\boldsymbol{\tau} = (\sigma_x, \sigma_y, \sigma_z)$ and $\boldsymbol{d}(k) = (0, -\Delta sink, -tcosk - \mu)^T$. Now keeping μ, t and Δ fixed and let k span the Brillouin zone $(0, 2\pi)$ we plot the vector $\boldsymbol{d}(k)$ on the $\tau_z - \tau_y$ plane.

Figure 3.1 illustrates the winding of the vector $\boldsymbol{d}(k)$ for three different values of the chemical potential. By changing the chemical potential we shift the center of the circle on the τ_z axis, while the sign of the superconducting coupling indicates the direction of the winding as k changes. For $\Delta > 0$ the direction is counter clockwise while for$\Delta < 0$ the opposite. The winding invariant is given by the number of revolutions of $\boldsymbol{d}(k)$ around the origin. For $|\mu| > t$ the circle does not include the origin so $\mathbb{Z} = 0$ (trivial phase), for $|\mu| < t$ the circle includes the origin and the invariant can take the values $\mathbb{Z} = \pm 1$ depending on the sign of Δ and finally for $\mu = t$ the circle is tangent to the τ_y-plane and the invariant cannot be defined. Note here that the vector traces out a circle in our examples since we have taken $t = \Delta$, in general the shape will be an ellipse but the arguments remain the same.

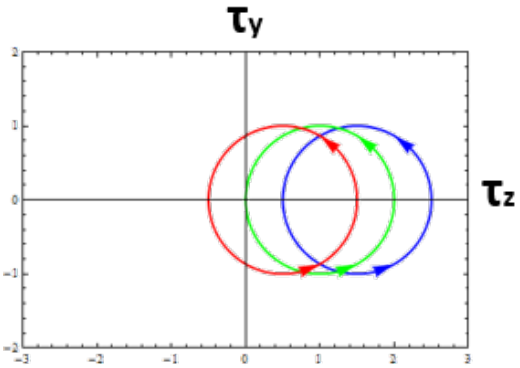

Figure 3.1: Winding of the vector $\boldsymbol{d}(k)$ *as* $k \in (0, 2\pi)$, $t = \Delta = 1$ *and* $\mu = -1.5$ *(blue),* $\mu = -1.0$ *(green),* $\mu = -0.5$ *(red).*

Chapter 4

Three topological wires

Our goal in this chapter is to investigate what happens when we bring the ends of three Kitaev chains close together forming a tri-junction. More specifically we are interested in how the zero modes that are sitting in the center of the junction interact with each other. Before doing so though it is instructive to exploit the properties of a different setup, namely those of a single Kitaev chain in which the superconducting coupling changes sign somewhere along the chain effectively forming a junction, which we will call π-junction.

4.1 π-junction

In the previous chapter we saw that the Kitaev Hamiltonian, depending whether t and Δ are real or imaginary, can be classified into the BDI or D symmetry class respectively. The superconducting order parameter has the form $\Delta = |\Delta|e^{i\phi}$, so if we want to let it change sign along the chain we have two options. Either we can set $\phi = 0$ and vary Δ which in this case is real (real π-junction), or we can vary the superconducting phase ϕ (phase winding π-junction). Due to symmetry considerations these two cases are fundamentally different. If Δ is real the Hamiltonian belongs to the BDI class where we have a $\mathbb{Z}$ invariant which can take the values $+1, 0, -1$. So if we let Δ smoothly vary from a positive to a negative value (assuming $|\mu| < 2t$) our system will go through a topological phase transition and the topological invariant will change its value from $+1$ to -1. The bulk-boundary correspondence, which holds for the free fermionic Hamiltonians that belong to the classification table 3.1, relates the number of edge mode with the change in the topological invariant, namely in the boundary between two regions that have topological invariants q and p, we expect $|q-p|$ gapless modes to emerge. Thus when we vary the superconducting phase no zero mode is present in the center of the π-junction as the topological invariant remains the same, in contrast to the case where Δ is purely real and two modes appear at the center of the π-junction. These two modes remain at zero energy and do not gap out since they belong to different topological phases.

The width of the junction is defined as the finite segment of the Kitaev chain in which the variation of the parameters (Δ or ϕ) takes place. It has been shown [29], that in the case of a phase winding junction, when we shrink the width of the junction, sub-gap states that "move" towards zero energy appear in the spectrum. In the limit where the width of the junction goes to zero (in our discrete model zero corresponds to one lattice spacing) the phase winding junction is effectively the same as the real junction and there are two zero modes localized at the "center" of the junction.

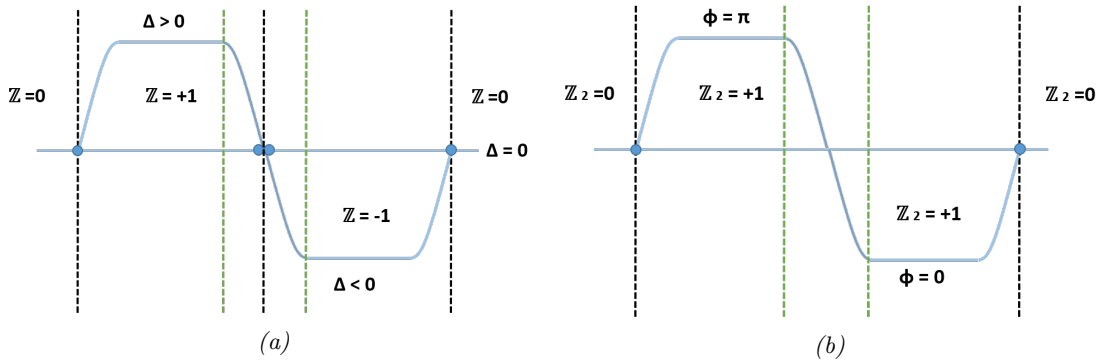

Figure 4.1: (a) A particular profile for a real Δ, we can see that the π-junction is formed by linearly decreasing Δ and that two Majorana modes (blue circles) are localized in the center of the junction where the topological invariant changes value. (b) Phase winding junction profile, in this case only the edge modes at the two ends of the chain are present. In both pictures the black dashed lines separate the different topological regions, while the green dashed lines indicate the width of the junction.

4.2 tri-junction

Now having in mind the basic properties of the π-junction that we briefly described in the previous section let us introduce the tri-junction setup. The tri-junction or T-junction, where the ends of three Kitaev wires are brought close together, has been studied in [2] and has been proposed as a platform for braiding the Majorana modes of the one-dimensional model. We want to focus on how the zero modes that are now sitting in the center of this junction interact with each other. Of course this strongly depends on how we couple the three wires in the center, so let us first explain how we construct the pertinent Hamiltonian matrix.

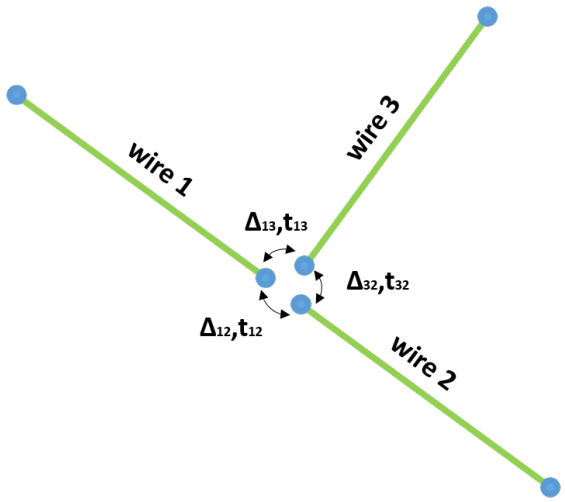

Figure 4.2: trijunction

Imagine the general case in which we have three topological wires each consisting of N_i, $i = 1, 2, 3$ number of sites. The Hamiltonian matrix will be a $(2N_1+2N_2+2N_3)\times(2N_1+2N_2+2N_3)$ matrix. Thus it will be a sparse block diagonal matrix formed by three matrices like the one that was introduced in chapter two, 2.10. The only thing that we have to do to make the three ends of the wires "talk" to each other is to add some off-diagonal terms that describe the coupling between these three sites. In our model we have two kinds of couplings for adjacent sites, the hopping t and the superconducting coupling Δ. So the matrix takes the following form:

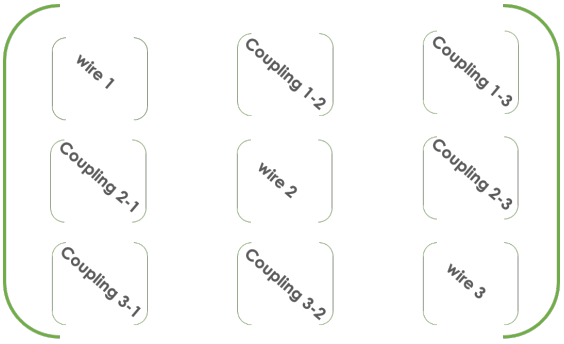

Figure 4.3: Hamiltonian matrix for the tri-junction

As we mentioned before the off-diagonal matrices that contain the coupling elements, connect only the three sites that are located at the ends (or the beginning depending on the convention) of the chains. However when we introduce the connections between the three wires we have to be careful and take into account the direction of the superconducting coupling that is induced due to the p-wave nature of the superconducting order parameter. Let us become more specific by considering some examples, starting with the case in which only two wires are coupled together.

In this case the Hamiltonian matrix consists only by the four blocks in the upper left corner of Figure 4.3. From equation 2.1 we can write down the terms that describe the coupling between the last site of the first wire (N_1) and the first site of the second wire ($N_1 + 1$):

$$\mathcal{H}_c = -\frac{t_{12}}{2}(c^\dagger_{N_1} c_{N_1+1} + c^\dagger_{N_1+1} c_{N_1}) - \frac{|\Delta_{12}|}{2}(e^{i\phi_{12}} c_{N_1} c_{N_1+1} + e^{-i\phi_{12}} c^\dagger_{N_1+1} c^\dagger_{N_1}) \tag{4.1}$$

As you can notice in the above equation we have assumed that the parameters t_{12} and $|\Delta|_{12}e^{i\phi_{12}}$ are independent from the hopping amplitudes and the superconducting order parameters of each wire, which is the most general expression we can write down in order to describe the coupling between the two wires. We note that often one sets $|\Delta_{12}| = 0$, but we do not do that. However, we will assume that t_{12} is real, without loss of generality. If we use equation 2.3 to write the fermionic operators in terms of the Majoranas and keep only the terms that describe the coupling between γ_1 and γ_2 we get:

$$\mathcal{H}_{\gamma\gamma} = -i\frac{t_{12}}{4}\cos\Big(\frac{\phi_1 - \phi_2}{2}\Big)\gamma_1\gamma_2 - i\frac{|\Delta_{12}|}{4}\cos\Big(\phi_{12} - \frac{\phi_1 + \phi_2}{2}\Big)\gamma_1\gamma_2 \tag{4.2}$$

where ϕ_1 and ϕ_2 are the phases of the superconducting coupling in wire 1 and 2 respectively. In general even when the two wires are weakly coupled the Majorana modes at the two ends split, acquiring a finite energy and form a "normal" fermion. However there are some special cases where this does not happen and even though the two wires are strongly coupled, the Majorana modes remain at zero energy.

First of all by looking at equation 4.2 one can see that there is a fine-tuned case where we can set $t_{12} = -|\Delta_{12}|$ and select the phases in such a way that the two terms cancel each other. For example if $\phi_1 = -\phi_2 = \pi$ and $\phi_{12} = 0$ the coupling between γ_1 and γ_2 is zero and the two modes remain at zero energy. Furthermore if a phase winding π-junction is formed, then from the previous section, we know that because the width of the junction is minimal the zero modes will persist. This is the case if, for instance, $\phi_1 = \pi$, $\phi_2 = 0$ and $\phi_{12} = \pi$ or 0, as you can see from equation 4.2 the values of t_{12} and Δ_{12} do not matter since the two terms will always be zero. Finally the last case corresponds to the formation of a real π junction between the two wires, so in this case the superconducting phases are zero and Δ changes sign in between the two wires. In this case we have argued that the two zero modes are topologically protected.

Now let us consider the case where all three wires are coupled together, the important thing to keep in mind is that the p-wave pairing has a particular direction in each wire. Notice that in equation4.2 the hopping term is symmetric in the exchange of the indices n and $n+1$ while the second term that describes the superconducting coupling is not, this is why there is a particular direction in the coupling. In the tri-junction case, the Hamiltonian that describes the coupling

between the three zero modes that sit in the center of the junction is obtained by following the same procedure as before:

$$\begin{aligned}\mathcal{H}_{\gamma_1\gamma_2\gamma_3} = &-i\frac{t_{12}}{4}\cos\Big(\frac{\phi_1-\phi_2}{2}\Big)\gamma_1\gamma_2 - i\frac{|\Delta_{12}|}{4}\cos\Big(\phi_{12}-\frac{\phi_1+\phi_2}{2}\Big)\gamma_1\gamma_2\\ &-i\frac{t_{13}}{4}\cos\Big(\frac{\phi_1-\phi_3}{2}\Big)\gamma_1\gamma_3 - i\frac{|\Delta_{13}|}{4}\cos\Big(\phi_{13}-\frac{\phi_1+\phi_3}{2}\Big)\gamma_1\gamma_3\\ &-i\frac{t_{23}}{4}\sin\Big(\frac{\phi_2-\phi_3}{2}\Big)\gamma_2\gamma_3 + i\frac{|\Delta_{23}|}{4}\sin\Big(\phi_{23}-\frac{\phi_2+\phi_3}{2}\Big)\gamma_2\gamma_3\end{aligned} \tag{4.3}$$

As you can notice, the third line of the equation differs from the above two, we will explain why this happens by describing how we couple the three wires step by step. To illustrate how the wires are coupled we draw the three wires in figure 4.4 and above them we draw arrows that point in the direction of the p-wave pairing.

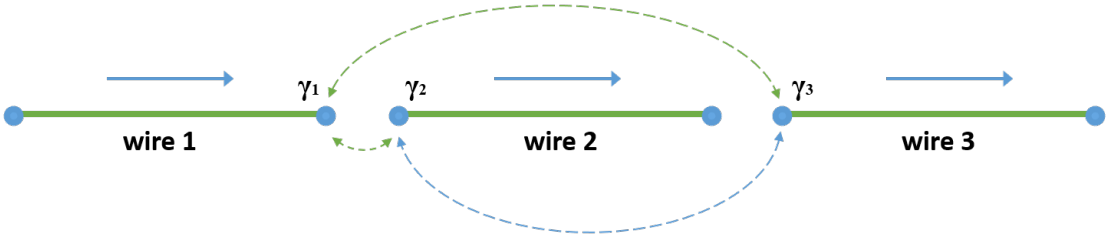

Figure 4.4: Direction of the p-wave coupling for the tri-junction setup. The dashed lines illustrate the coupling between the Majorana zero modes while the blue arrows show the direction of the pairing.

Starting with the first wire we assume that the site indices increase when we move from left to right, this is what gives the direction of the pairing. So when we want to connect the right end of wire 1 with the left end of wire 2, we have to keep in mind that because the direction of the pairing in wire 1 points into the junction, the direction of the pairing in wire 2 must point away from the junction. The same thing happens when we connect the right end of the first wire with the left end of the third wire. However an ambiguity arises when we now try to establish the final connection between wires 2 and 3, in these two wires the direction of pairing is fixed based on their already established connection with the first wire. Thus when we connect these two wires because the direction of the pairing in both wires points away from the junction the coupling between them will differ. So in this setup it is inevitable to form a connection between two wires that is different from the other two.

In general two of the zero modes that sit in the center of the tri-junction will combine forming a finite energy fermion and only one Majorana mode will remain. Still, let us consider a case where, even though all wires are connected to each other, the three Majorana modes in the center of the junction remain at zero energy. For simplicity we will assume that all the parameters of the model are real; then one would expect that the three modes would remain at zero energy if we would create real π-junctions between all pairs of wires. However, it turns out that we only need to create a real π-junction between wire 1 and 2 and between wire 1 and 3, since there is an already built in π difference between the second and the third wire due to their different coupling.

Chapter 5

Transport theory

Here our goal is to extract the relations for calculating the conductance and the density of states for the Kitaev chain and then develop a numerical implementation. In order to do so, we will use the concept of the Green's functions which, for the non-interacting case, is related to the scattering matrix approach. The approach we will consider is very useful when dealing with arbitrary shaped conductors. We will review the most important concepts of the formalism for a normal conductor, by closely following Datta's book [7], and then we will explain how the situation changes when we are dealing with a superconductor.

5.1 Transport through a normal tight binding chain

Let us forget for a moment that our system is a superconductor and see how the formalism works for a simple one-dimensional tight binding chain; we will not derive any of the relations here but we will highlight the important details, as one can find a more detailed description in [7].

The time independent or energy dependent Green's function gives us the response at any point x due to an excitation at any other point x' and when the response is related to the excitation by a differential operator the Green's function can be written as the inverse of the operator. In order to calculate the transmission through a finite tight binding chain we have to connect semi-infinite leads at the two ends of our chain.

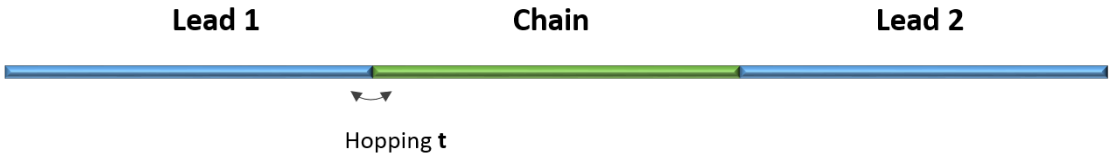

Figure 5.1: Tight-binding chain with two leads attached

When interactions in the chain are not taken into account the only excitations we are interested in are those coming from the semi-infinite leads and the Green's function allows us to calculate the transmission probability of a wave incident from one of the leads. In our case the Green's function takes the following form:

$$G = (E - \mathcal{H})^{-1} \tag{5.1}$$

where $\mathcal{H}$ is the Hamiltonian operator and E the energy of the incident wave. However in order to uniquely determine the inverse of a differential operator we have to take into account the boundary conditions. The two Green's functions that correspond to different boundary conditions are usually called advanced and retarded.

For a simple one-dimensional chain the advanced Green's function $G(x, x')$ corresponds to two waves that travel towards the excitation point while the retarded one to those that travel

outwards. One way to include the boundary conditions into equation 5.1 is by adding an infinitesimal $i\epsilon$ term to the energy. If this term is positive the advanced function grows indefinitely towards infinity and the only acceptable solution is the retarded one, while when the term is negative the opposite thing happens.

The tight binding Hamiltonian matrix for a normal one-dimensional wire takes the usual form:

$$\begin{pmatrix} -\mu & -t & & & \\ -t & -\mu & -t & & \\ & -t & -\mu & -t & \\ & & \ddots & \ddots & \ddots \end{pmatrix} \tag{5.2}$$

So in order to obtain the retarded Green's function we just have to set up the matrix $[(E+i\epsilon)I-H]$ and invert it.

$$G^R = [(E + i\epsilon)I - H]^{-1} \tag{5.3}$$

The problem in this case is that, because the semi-infinite leads have to be taken into account, the Hamiltonian matrix becomes infinite dimensional. To overcome this difficulty the matrix has to be truncated, in this process it is assumed that only the last (or first) site of the semi-infinite leads is coupled to the chain and the effect of the leads is taken into account by adding self energy terms in the diagonal of the chain's Hamiltonian matrix. More specifically, for the setup illustrated is figure 5.1 a self energy term for lead 1 has to be added in $H(1,1)$ while another term for lead 2 has to be added in $H(N,N)$ where N is the number of sites of the chain.

The self energy terms describe the interaction between the leads and the chain and are given by $\Sigma_i^R = t_{couple}^2 g_l^R$, where $i = 1, 2$, t_{couple} is the coupling between the chain and the leads and g_l^R the Green's function for the semi-infinite lead [8]. The Green's function for an one-dimensional semi-infinite tight-binding chain can be analytically calculated using the eigenfunction expansion of the Green's function at the closed boundary of the chain [26] and is given by the following relation:

$$g_l^R = \begin{cases} \frac{1}{2t_{lead}^2}(E + \mu + i \cdot sgn(E+\mu)\sqrt{4t_{lead}^2 - (E+\mu)^2}) & \text{,if } E > 2t_{lead} \\ \frac{1}{2t_{lead}^2}(E + \mu - i\sqrt{4t_{lead}^2 - (E+\mu)^2}) & \text{,else} \end{cases} \tag{5.4}$$

Thus, the retarded Green's function of the full system (leads+chain) will be:

$$G^R = [EI - H_c - \Sigma^R]^{-1} \tag{5.5}$$

Note here that by adding the self energy terms we can introduce an effective Hamiltonian $\mathcal{H}_{eff} = H_c + \Sigma^R$ which is not Hermitian, since $\Sigma^R \neq (\Sigma^R)^\dagger = \Sigma^A$. As a result, the eigenvalues of this Hamiltonian are complex numbers and can be written in terms of the eigenvalues ϵ_c of the original Hamiltonian (without the leads).

$$\epsilon_c' = \epsilon_c - \delta\epsilon - i\gamma \tag{5.6}$$

The real part $\delta\epsilon$ describes an energy shift that is induced when we add the leads, while the imaginary part describes the fact that the electrons can escape into the leads. If we consider the time evolution of the state and square the wavefunction to obtain the probability we end up with:

$$|\psi_c|^2 e^{-\frac{2\gamma t}{\hbar}} \tag{5.7}$$

The quantity $\hbar/2\gamma$ can be seen as the lifetime of the state before leaking out into the leads [7].

5.1.1 Spectral function

A very important concept of this formalism is the one of the spectral function that is defined in the following way:

$$A = i[G^R - G^A] \tag{5.8}$$

we can think of this function as a matrix version of the density of states since by taking the diagonal elements of the matrix we obtain the local density of states:

$$\rho(i;E) = \frac{1}{2\pi}A(i,i;E) = -\frac{1}{\pi}Im[G^R(i,i;E)] \tag{5.9}$$

while by taking the trace we get the total density of states:

$$N(E) = \frac{1}{2\pi}Tr[A(E)] \tag{5.10}$$

The total density of states gives the number of states as a function of the energy, while the local density of states gives the density of states as a function of the spatial coordinate. Knowing that, $Im(\frac{1}{x+i0^+}) = -\pi\delta(x)$ we can easily notice that the spectral function and the local density of states, as functions of the energy ω, will be a collection of delta functions centered around the eigenvalues of the system. One problem arises when we try to simulate our system using numerical methods, namely in order to obtain the local density of states of our system, as a function of the energy, we scan an energy interval with a finite intermediate step. As a result it is natural to miss some energy values that correspond to the eigenvalues of the system and thus these states remain "invisible".

However as we saw before, when we attach the leads to the system the eigenvalues become complex and more specifically the δ-peaks get shifted by $\delta\epsilon$ and get broadened because they acquire finite lifetime (because of the imaginary part). So because of the broadening it is now possible to "see" these states and the problem is resolved. In the case where no leads are present we can introduce "by hand" an infinitesimal $i\epsilon$ that broadens the peaks and sometimes even when the leads are present, introducing this artificial term leads to more efficient results.

5.1.2 Transmission formula

As we mentioned before the concepts of the S-matrix and of the Green's function are closely related and as Datta also points out, in the non-interacting case, which formalism one uses is mostly a matter of taste. The Fisher-Lee formula is a relation that connects the elements of the S-matrix with the Green's function:

$$s_{ij} = -\delta_{ij} + i\hbar\sqrt{v_i v_j}G^R_{ij} \tag{5.11}$$

where $v_i = \frac{\hbar k}{m}$ the velocity in lead i. By using the above formula and knowing that $T_{ij} = |s_{ij}|^2$, the transmission probability from lead i to lead j can be written in terms of the Green's functions [7]:

$$T_{ij} = Tr[\Gamma_i G^R \Gamma_j G^A] \tag{5.12}$$

The elements of gamma matrices are given by $\Gamma_i = i(\Sigma^R_i - \Sigma^A_i)$ and are usually called broadening functions since they are analogous to the imaginary part of the self energies. We have to note here that equation 5.12 only holds for $i \neq j$. For $i = j$ we have to modify it in the following way:

$$T_{ii} = 1 + Tr[\Gamma_i G^R \Gamma_i G^A + 2\Gamma_i Im(G^R)] \tag{5.13}$$

5.2 Doubling the problem

To generalize the formalism for the case of the Kitaev chain, based on Datta's approach for dealing with superconducting systems [9], we will split each normal lead into two, one electron lead and one hole lead. So in this case self energy terms have to be added for both electrons and holes. The Green's function for the electron semi-infinite lead will be calculated as before from equation 5.4 while for the hole lead it will be $g^R_{l,h}(E) = -[g^R_{l,e}(-E)]^\dagger$.

To better illustrate the form of the Green's function matrix let us consider a three site Kitaev chain with two semi-infinite leads attached at the two edges, the matrix in this case is:

$$\begin{pmatrix} E+\mu+\Sigma^R_{1,e} & t & 0 & 0 & -\Delta e^{-i\phi} & 0 \\ t & E+\mu & t & \Delta e^{-i\phi} & 0 & -\Delta e^{-i\phi} \\ 0 & t & E+\mu+\Sigma^R_{2,e} & 0 & \Delta e^{-i\phi} & 0 \\ 0 & \Delta e^{i\phi} & 0 & E-\mu-\Sigma^R_{1,h} & -t & 0 \\ -\Delta e^{i\phi} & 0 & \Delta e^{i\phi} & -t & E-\mu & -t \\ 0 & -\Delta e^{i\phi} & 0 & 0 & -t & E-\mu-\Sigma^R_{2,h} \end{pmatrix}^{-1} \tag{5.14}$$

The indices of the self energies correspond to the number of the lead (1,2) and the electron or hole lead (e,h) respectively. If we would like to calculate the density of states a small $i\epsilon$ should be added in the diagonal elements in order to broaden the states. For the same example the gamma matrices for the two leads are:

$$\Gamma_1 = \begin{pmatrix} i(\Sigma_{1,e}-\Sigma^\dagger_{1,e}) & 0 & 0 & 0 & 0 & 0 \\ 0 & 0 & 0 & 0 & 0 & 0 \\ 0 & 0 & 0 & 0 & 0 & 0 \\ 0 & 0 & 0 & i(\Sigma_{1,h}-\Sigma^\dagger_{1,h}) & 0 & 0 \\ 0 & 0 & 0 & 0 & 0 & 0 \\ 0 & 0 & 0 & 0 & 0 & 0 \end{pmatrix} \tag{5.15}$$

$$\Gamma_2 = \begin{pmatrix} 0 & 0 & 0 & 0 & 0 & 0 \\ 0 & 0 & 0 & 0 & 0 & 0 \\ 0 & 0 & i(\Sigma_{2,e}-\Sigma^\dagger_{2,e}) & 0 & 0 & 0 \\ 0 & 0 & 0 & 0 & 0 & 0 \\ 0 & 0 & 0 & 0 & 0 & 0 \\ 0 & 0 & 0 & 0 & 0 & i(\Sigma_{2,h}-\Sigma^\dagger_{2,h}) \end{pmatrix} \tag{5.16}$$

The transmission probability from the left lead to the right will be given again by equation 5.12 with the only difference being that in this case we are dealing with $2N \times 2N$ matrices.

5.3 Conductance

In order to obtain the formula for the conductance we will use the Laudauer-Buttiker formalism[19] [6], which describes the coherent transport through multi-terminal conductors. The semi-infinite leads are treated as particle reservoirs and it is assumed that the particles escape from the conductors without being reflected and that we are in the ballistic regime. In this formalism the current in lead i is given by:

$$I_i = \frac{e}{h}\sum_j \int \Big(f_j(E) - f_i(E)\Big) T_{ij}(E) dE \tag{5.17}$$

Where $f(E)$ the Fermi distribution function and T_{ij} the transmission probability. So the current in lead i is basically given by the transmission probabilities for an electron to tunnel from lead i to lead j weighted by the Fermi functions. Let us now consider two different setups and see how, by using the current formula, we can obtain the conductance.

5.3.1 NS junction

First let us attach only one lead to our superconducting wire, thus forming a normal-superconductor (NS) interface. We split the normal lead into an electron and a hole lead and a voltage difference

is applied between the superconductor and the normal lead. For simplicity we will assume that the chemical potential in both parts is equal to zero. The current in the electron lead takes the following form:

$$I_{ne} = \frac{e}{h}\int_0^\infty dE\Big[\Big(f_{se}(E) - f_{ne}(E)\Big)T_{ne,se}(E) + \big(f_{sh}(E) - f_{ne}(E)\Big)T_{ne,sh}(E) + \Big(\big(f_{nh}(E) - f_{ne}(E)\Big)T_{ne,nh}(E)\Big] \tag{5.18}$$

Where by ne we denote the normal electron lead and by se,sh the electrons and holes in the superconductor. The first two terms correspond to the cases where an electron from the normal region has bigger, or smaller, energy from the energy gap and thus becomes a superconducting electron, or a hole, respectively. The third term that describes the reflection of a normal electron as a hole, corresponds to a subgap physical processes that can take place in a NS interface. We will concentrate in this process in the next chapter, for now we just apply equation 5.17 to our setups. The flux conservation requires that $T_{ne,nh} + T_{ne,ne} + T_{ne,se} + T_{ne,sh} = 1$ and by using it we can express the transmission probabilities $T_{ne,se}$, $T_{ne,sh}$ in terms of the other two, that can be calculated from the formalism that we have already developed. For example $T_{ne,nh}$ is given by:

$$T_{ne,nh} = Tr[\Gamma_{ne} G^R \Gamma_{nh} G^A] \tag{5.19}$$

In the above relation the gamma matrices Γ_{ne}, Γ_{nh} contain only the self-energy terms that have to do with the electrons and the holes respectively. Following the same line of thought we can obtain the expression for the hole current in the normal part I_{nh} and the total current will be given by $I = I_{ne} + I_{nh}$.

The conductance is the derivative of the current with respect to the applied voltage:

$$\mathcal{G}_c = \frac{\partial I}{\partial V} = \frac{\partial (I_{ne} + I_{nh})}{\partial V} \tag{5.20}$$

If we assume zero temperature the Fermi functions in the current expression become theta functions and we conclude that the conductance for the NS junction will be:

$$\mathcal{G}_{NS} = \frac{e^2}{h}[1 - T_{ne,ne} + T_{nh,ne}] \tag{5.21}$$

5.3.2 NSN junction

In this case two leads are attached to the ends of the superconductor and a voltage difference is induced between the left and the right lead. In figure 5.2 we sketch the NSN setup where the two normal leads have been split into electrons and holes as usual.

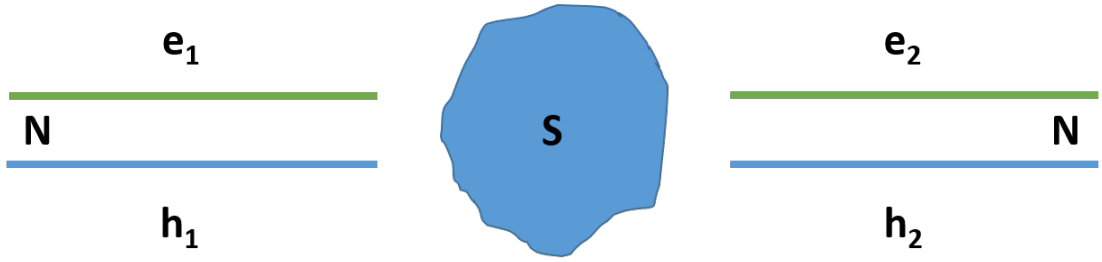

Figure 5.2: NSN junction

The current in the left electron lead will be given by:

$$I_{e1} = \frac{e}{h}\int_0^\infty dE\Big[\Big(f_{e2}(E) - f_{e1}(E)\Big)T_{e1,e2}(E) + \big(f_{h2}(E) - f_{e1}(E)\Big)T_{e1,h2}(E) + \Big(\big(f_{h1}(E) - f_{e1}(E)\Big)T_{e1,h1}(E)\Big] \tag{5.22}$$

The flux conservation will be $T_{e1,h1}+T_{e1,h2}+T_{e1,e1}+T_{e1,e2}=1$ and with the same argumentation as before the conductance is:

$$\mathcal{G}_{NSN}=\frac{e^2}{h}[1-T_{e1,e1}+T_{h1,e1}] \tag{5.23}$$

The derivation of the above result is given in Appendix A, again we will review the physical processes that correspond to each term of the current formula in the following chapter.

Chapter 6

Numerical results

The formalism that was developed in the previous chapter is very handy when it comes to the numerical implementation. We will first use the formalism to review a local process that takes place in a normal (N), superconducting (S) interface and explain how the presence of a Majorana zero mode affects the conductance spectrum. Then we will present some numerical results for the NSN junction for different profiles of the superconducting order parameter.

6.1 Perfect Andreev refection

Let us imagine the following setup, say we couple a normal region with a superconductor, forming a NS interface and we let current flow from the normal region to the superconducting one. If the energy of the incoming electrons is bigger (or smaller) than the energy gap there are accessible electronic states on the superconductor and the electrons can tunnel into them, while in the subgap region this is not the case. So one would naively think that in the subgap region all electrons are reflected back into the normal region.

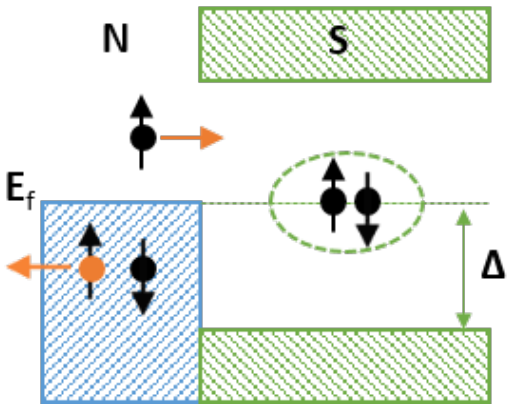

Figure 6.1: Andreev reflection in an s-wave sperconductor.

However because of the Cooper pair condensate that sits at zero energy there is another process that can occur (see figure 6.1), namely an electron with energy E can "draw" another electron with energy -E and opposite spin, forming a Cooper pair inside the superconductor and a hole is reflected back into the normal region, this process is called Andreev reflection. As a result inside the superconductor the electron current is converted into supercurrrent, carried by Cooper pairs. It has been shown [5] that when the NS interface is perfectly transparent the probability of the Andreev process goes to 1 in the subgap region. On the other hand, if we introduce a potential barrier on the interface, thus making it less transparent, and gradually increase the strength of the barrier, the probability of the Andreev reflection is suppressed.

For the case of a p-wave superconductor in the topological phase, the situation changes

drastically because of the Majorana zero mode that is now present at the boundary. Let us consider a setup like the one illustrated in figure 5.1 but with only the left lead attached to the chain. Moreover we make the Kitaev chain sufficiently long, so that the interaction between the two zero modes can be neglected. As we have mentioned before the lead couples to the chain with a t_{couple} hopping amplitude, therefore the case where $t_{couple} = t_{lead} = t_{chain}$, corresponds to a perfectly transparent NS interface, while decreasing the t_{couple} is similar to the introduction of a potential barrier on the interface. The normal lead, as we pointed out in the previous chapter, splits into an electron and a hole lead and so, after adding the appropriate self-energy terms and constructing the gamma matrices for this case, we can numerically calculate the probability of the process in which an electron is reflected as a hole:

$$T_{eh} = Tr[\Gamma_e G^R \Gamma_h G^A] \tag{6.1}$$

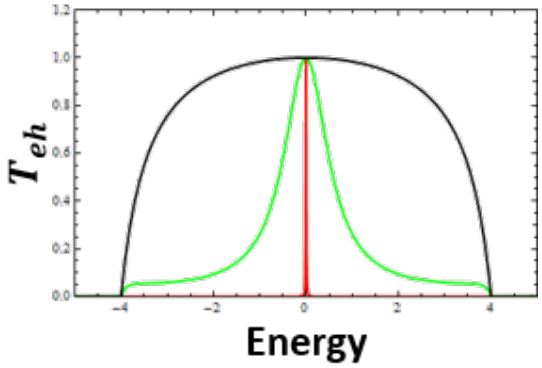

Figure 6.2: Andreev reflection probability as a function of the energy for a chain consisting of 42 *sites, with* $\Delta = 4.0$ *and for three different values of the tcouple parameter. Black:* $tcouple = tlead = tchain = 4.0$*, green:* $tlead = tchain = 4.0$*,* $tcouple = 2.0$*, red:* $tlead = tchain = 4.0$ *and* $tcouple = 0.2$*.*

In figure 6.2 the probability for the Andreev process is depicted for three different values of t_{couple}. As t_{couple} decreases you can see that the probability is suppressed in the whole subgap region except at zero energy where it stays fixed at 1. The conductance can be calculated from equation 5.21 and for the case where the coupling between the lead and the chain is weak we can see (figure 6.3) a peak at zero bias with a maximum of $2e^2/h$. Note that in the realistic model that was introduced at the end of the second chapter, superconductivity was induced into the wire by proximity, as the wire is placed next to an s-wave superconductor. Thus in this case the conductance is measured between the lead and the bulk s-wave superconductor.

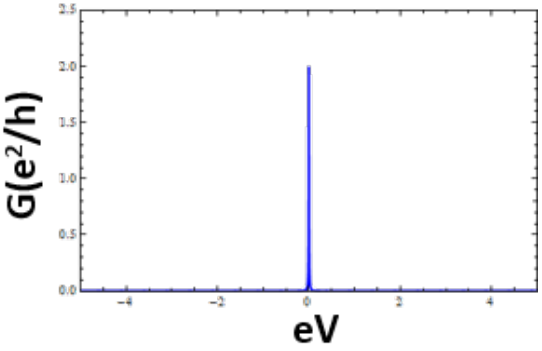

Figure 6.3: Conductance for a weakly coupled NS junction with $N = 42$ *sites* $tchain = tlead = 4.0$ *and* $tcouple = 0.2$*.*

The zero bias peak appears because of the Majorana mode, as the state that is now sitting on zero energy leads to resonant transmission. This has been argued to be a characteristic signature

of a Majorana zero mode and many experimental groups have verified the existence of a zero bias peak in similar setups that have tried to reproduce the above behavior. Nevertheless, as it has already been pointed out in the introduction, there are also other effects one has to take into account that can produce a similar zero bias peak, thus the observation of the zero-bias peak cannot be considered as a smoking gun evidence for the existence of the Majorana zero modes.

Furthermore we can simulate and examine how the probability of the Andreev process changes when we bring the zero modes of the Kitaev chain close to each other, by reducing the length of the chain and move away from the fine-tuned limit ($\mu = 0$ and $t = \Delta$) in which the two modes at the ends of the chain are not coupled to each other. The two modes in this case are coupled and form a normal fermionic mode with finite energy, this will lead to the splitting of the zero bias peak and the conductance will take the form that is illustrated in figure 6.4.

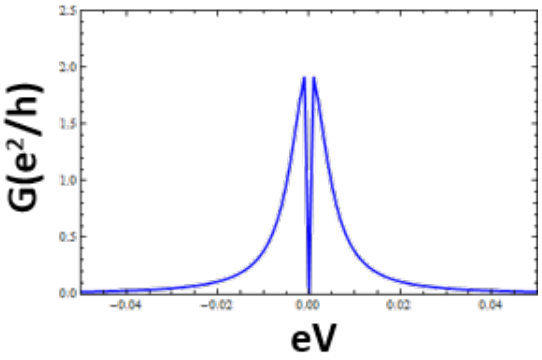

Figure 6.4: Conductance for a weakly coupled NS junction with tchain=tlead=4.0, tcouple=0.2, N=14 sites and $\Delta = 6.0$.

This is because, in this case there is no resonant Andreev reflection at zero voltage.

6.2 NSN junction

Let us now turn our attention to the NSN setup by connecting semi-infinite leads on both left and right of the Kitaev chain. Our goal is to investigate how and if the presence of the Majorana zero modes that exist between the two leads affect the conductance spectrum for three different profiles of the superconducting order parameter. Namely, at first we will examine the conductance through a Kitaev chain in which the superconducting order parameter takes a constant value along the chain and afterwards investigate the cases of a real π-junction and of a phase winding junction.

In order to understand the physical processes that can take place in the above setup let us say a few words concerning the three terms of the current formula 5.22 from which the conductance is derived. When using the LB formalism we formulate the current by taking into account all the possible transmission probabilities from the lead that we are interested in, to all the other leads that are connected to our setup. The first two terms correspond to an electron from the left side that tunnels into the electron and the hole lead on the right side, respectively. Both these two processes require that the length of the superconducting region will be sufficiently small and that a finite amplitude of the incident electron exists on the right side. The process where an electron can tunnel through the superconductor in the subgap region is called elastic co-tunneling (EC) and we can think of it as the tunneling of an electron through a virtual state that exists above the energy gap. While the process where an electron is transmitted as a hole on the right side is called crossed Andreev reflection (CAR) and can be seen as an electron forming a Cooper pair with an electron from the right side and a hole is reflected to the right hole lead. The transmission probability for the elastic co-tunneling can be calculated from equation 5.12 and is denoted as T_{ee}^{LR}, where the indices indicate the transmission of an electron from the left lead to right, while for the crossed Andreev process by T_{eh}^{LR}. Finally the last term corresponds to the local Andreev reflection T_{eh}^{LL} that was discussed at the beginning of this chapter.

6.2.1 Constant order parameter

By using the conductance formula 5.21, at first we calculate the conductance of a Kitaev chain where the superconducting order parameter increases gradually at the begining and then stays constant until it will go back to zero at the other end of the chain (see Appendix C.1). The exact profile of the order parameter is given in Appendix C. In figure 6.5 we can see the local density of states for the above setup together with the conductance as a function of the voltage. The local density of states is calculated by first constructing the Green's function matrix, then adding a small $i\epsilon$ term to the diagonal elements and using equation 5.9. In this case both leads are perfectly coupled to the chain, meaning that the NSN interface is perfectly transparent ($t_{lead} = t_{chain} = t_{couple}$). So when the energy of the incoming electron is bigger or smaller than the energy gap the conductance is equal to one, since there are accessible electronic states in the superconductor. While in the subgap region, as we have seen in the previous section, the conductance goes to 2 because the perfect Andreev reflection is the dominant process.

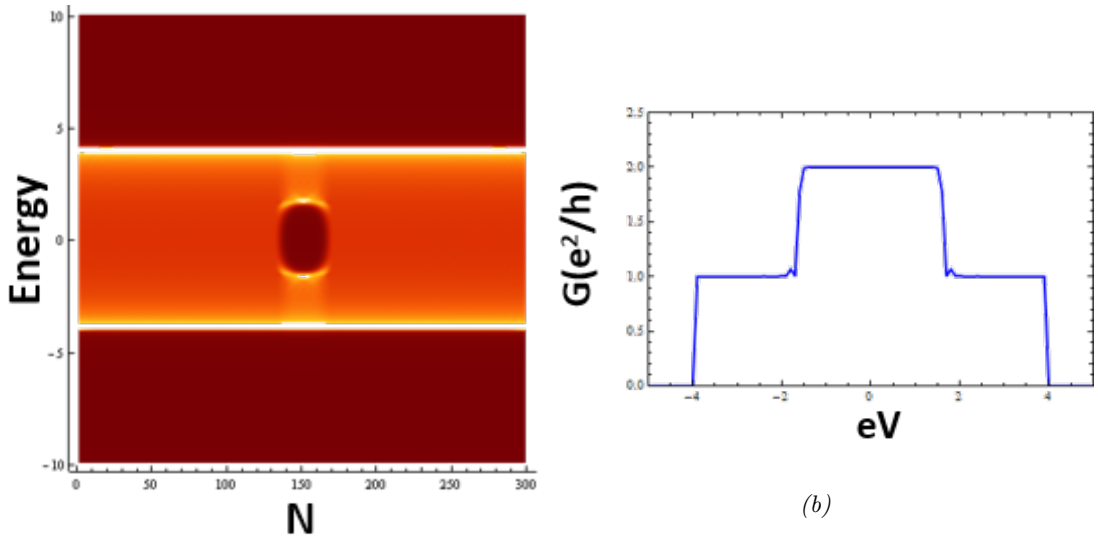

(a) *(b)*

Figure 6.5: The Kitaev chain in this case consists of 42 *sites, tcouple = tchain = tlead =* 4.0 *(perfect coupling) and* $\Delta = 1.6$. *(a) Local density of states of an NSN setup where the superconducting order parameter remains constant (for the exact profile see C.1). (b) Conductance as a function of the applied voltage.*

Now we can explore the weak coupling limit by decreasing the t_{couple} parameter which couples the leads with the chain. The conductance in this case is illustrated in figure 6.6 and as you can observe the zero bias peak that is connected to the presence of the Majorana zero mode remains, as one would expect from our previous discussion concerning the NS junction.

The only process that contributes to the zero-bias peak in figure 6.6 is the local Andreev reflection and no contributions come from the co-ellastic tunneling or the crossed Andreev process. We also have to note here that if we increase the length of the superconducting region, in both cases, the conductance plots remain the same. On the other hand if we decrease the length of the superconducting region, in the weakly coupled case, we observe the splitting of the zero bias peak.

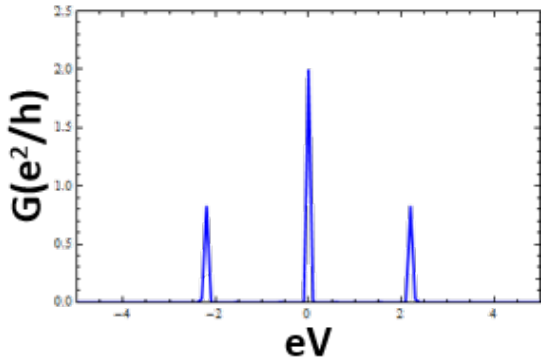

Figure 6.6: Conductance of the NSN junction with a constant superconducting order parameter profile $\Delta = 1.6, N = 42$ *sites, for the case where the leads are weakly coupled to the chain (tcouple* $= 0.2$ *and tlead* $=$ *tchain* $= 4.0$*).*

6.2.2 Real π-junction

We have seen that when the superconducting order parameter remains real and changes sign somewhere along the chain a π-junction is formed that supports two zero modes in its center. By assigning a profile like this (see Appendix C.2) to the superconducting order parameter we can plot the local density of states and the conductance for this case. In figure 6.9 at the local density of states plot, the white blob at zero energy depicts the two modes that are localized in the center of the junction and right next to it the conductance is plotted for $t_{lead1} = t_{couple1} = t_{chain}$; i.e. a perfectly transparent interface.

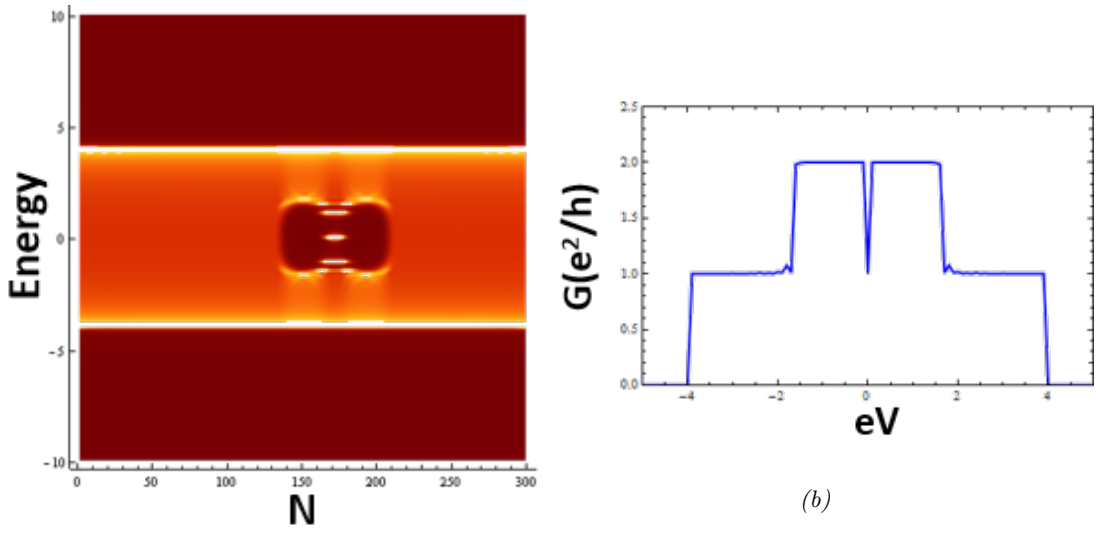

(a) *(b)*

Figure 6.7: Here the superconducting region consists of 84 *sites and the order parameter forms a real* π*-junction by changing from* $\Delta = 1.6$ *to* $\Delta = -1.6$*, the width of the junction is* 30 *sites long and the exact profile for the order parameter is given in Appendix C.2. (a) Local density of states of a real* π*-junction profile with tcouple* $=$ *tlead* $=$ *tchain* $= 4.0$*. (b) Conductance as a function of the voltage.*

As you can easily notice the conductance plot differs from the previous one, as in this case at zero bias the conductance is suppressed and is equal to 1 even for a perfectly transparent interface. Moreover when we decrease the $t_{couple1}$ parameter the conductance is suppressed everywhere and no zero bias peak is present in the weak coupling limit (figure 6.8).

The conductance in both cases was calculated for a superconducting region consisting of 84

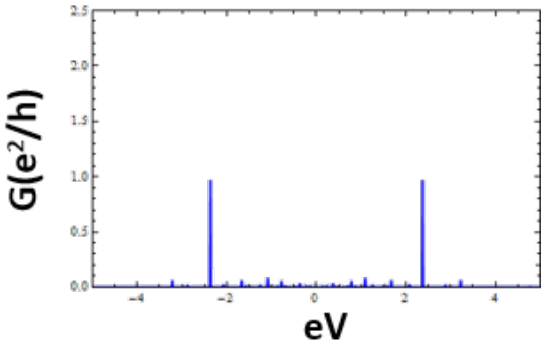

Figure 6.8: Conductance for the real π-junction in the weak coupling case (tchain=tlead=4.0 and tcouple=0.2).

sites. However, it was noticed that, if we furthermore increase the length of the superconducting region while keeping the length of the real π-junction fixed, the conductance behaves in the same way as for the constant order parameter case. Namely, when the leads are perfectly coupled with the chain, the conductance in the subgap region is constant and equal to 2, while for the weakly coupled leads the zero bias peak appears again in the spectrum. Thus there is a maximum length of the superconducting region beyond which the conductance behaves in a different way, of course this highly depends on the exact profile we have chosen for the superconducting order parameter, so there is nothing special about this particular length (84 sites).

In order to understand why such a dip is observed in the conductance at zero bias we can calculate separately the transmission probabilities for all the different processes that can take place and find out which are the ones that contribute to the conductance. Figure 6.9 depicts the transmission probability for an electron tunneling from the left to the right side of the Kitaev chain and the probability for the local Andreev process for a superconducting region consisting of 84 sites. The leads are perfectly coupled to the chain and as you can see at zero bias the transmission probability for an electron tunneling from left to right goes to one, as a result the probability for the local Andreev process is totally suppressed at this voltage, that is exactly why a conductance dip appears at zero bias. Also we observed that when the length of the superconducting region is increased, the zero bias peak in the T_{ee} plot gradually fades away while the probability of the Andreev process goes to one. Moreover it turns out that the real π-junction has to be placed exactly at the center of the superconducting region for the resonant transmission to occur otherwise when moving the junction away from the center the zero bias peak in the T_{ee} spectrum gradually goes to zero.

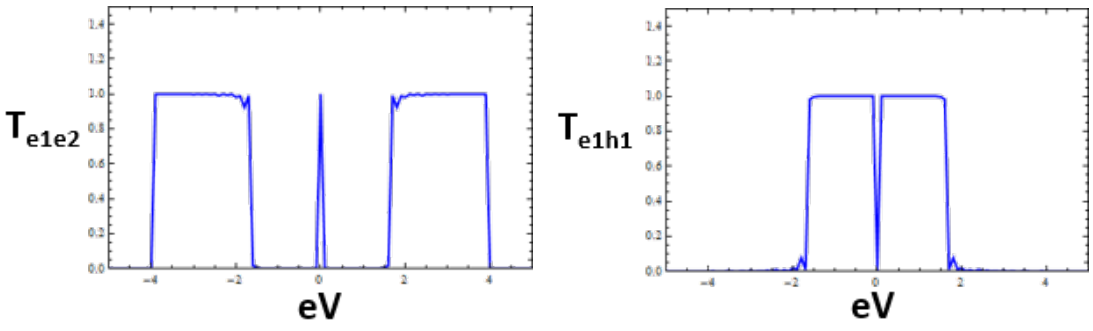

(a) *(b)*

Figure 6.9: (a) Transmission probability for an electron tunneling from the left lead to the right (co-elastic tunneling). (b) Transmission probability for the local Andreev process. Both transmission probabilities have been calculated for the perfectly coupled case where tchain = tlead = tcouple = 4.0.

So it turns out that the localization of a fermionic mode (composed of two Majorana zero modes) in the center of the junction allows for the resonant transmission of an electron through the Kitaev chain. For this process to occur, two necessary conditions have to be met; the length of the superconducting region should not exceed a maximum length and the π-junction has to be placed in the center of the superconducting region. Note that in the case of the constant order parameter where only two zero modes sit at the ends of the chain no such process was observed, even when the length of the superconducting region was "small".

6.2.3 Phase-winding junction

If we now keep the absolute value of the order parameter constant and instead vary the superconducting phase from 0 to π along the chain, we know that when the variation occurs gradually no zero modes are present at the center of the junction. Instead subgap bound states exist in this case, which are called Andreev bound states (ABS), however these states do not contribute to the conductance spectrum. As a result, the conductance in this case is similar to the one that we have numerically extracted for a constant order parameter (see figure 6.5(b)). If we shrink the length of the phase winding junction these ABS start to move towards zero energy and when a sudden variation (one lattice site) of the superconducting phase occurs, the conductance for a chain that is perfectly coupled to the leads, behaves as illustrated in figure 6.10. The dip at zero bias appears again because there is a resonant transmission at the T_{ee} channel and thus the local Andreev process is suppressed. When we increase the width of the phase winding junction, even by adding just one lattice site, the zero modes in the middle of the junction move slightly away from zero energy and the dip immediately disappears. Thus it seems that the resonant transmission of an electron tunneling through the chain is a very fine-tuned process that strongly depends on the fact that the zero modes sit exactly at zero energy.

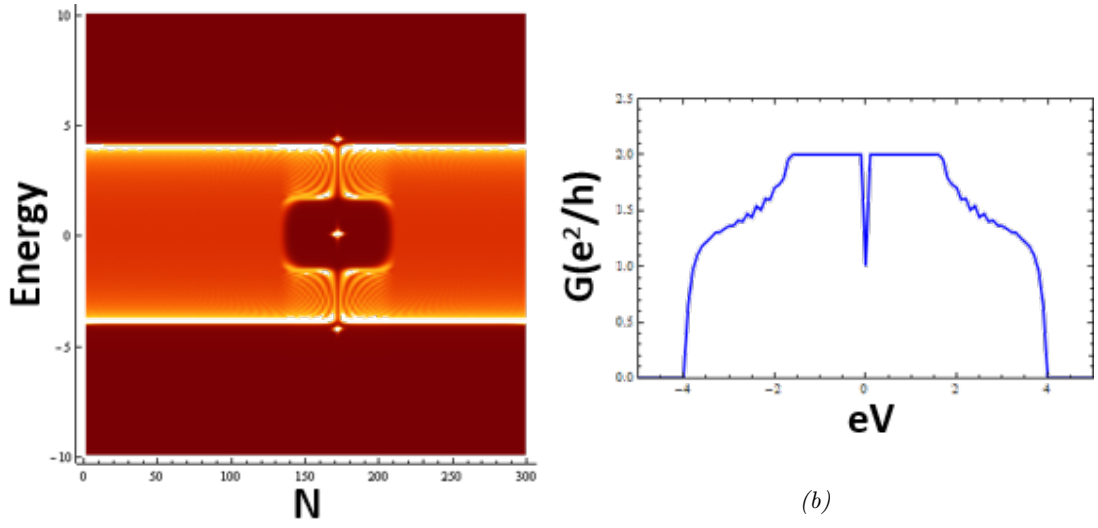

(a) (b)

Figure 6.10: The absolute value of the superconducting order parameter remains constant $|\Delta| = 1.6$ while the superconducting phase goes from π to 0 in the middle of the superconducting region (see Appendix C.3). (a) Local density of states for a phase-winding junction where a sudden variation of the superconducting phase occurs. (b) Conductance for the phase-winding junction for perfectly coupled leads $tcouple = tchain = tlead = 4.0$.

By looking at the conductance plot in figure 6.10, you can notice that besides the fact that there is no sharp step between the conductance for voltages inside and outside the subgap region, the dip at zero bias is again present. The fact that the conductance above and below the gap, is bigger than one and smoothly goes to two at the subgap region is because the probability for the local and the crossed Andreev process is non-zero even for voltages above and below the gap.

The transmission probabilities for all the processes that contribute to the conductance in this case are depicted in figure 6.11. This seems reasonable if you observe that in the local density of states plot on the lattice site where the sudden variation of the superconducting phase occurs, the electronic states above (or below) the gap are pushed towards bigger (or smaller) energies and as a result the gapped region is extended on this lattice site.

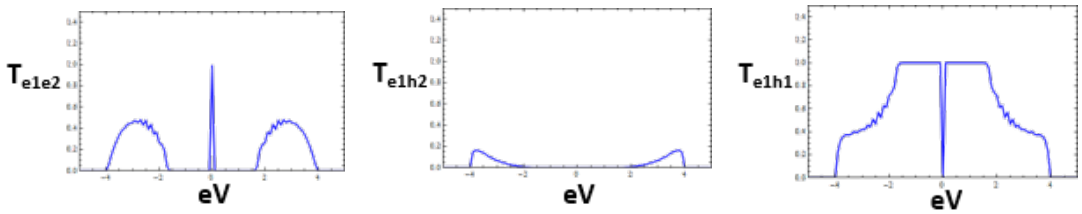

(a) *(b)* *(c)*

Figure 6.11: Transmission probabilities for (a) electron tunneling though the chain, (b) crossed Andreev reflection and (c) local Andreev reflection. These are the processes that contribute to the conductance of a perfectly coupled (tchain = tcouple = tlead = 4.0) phase-winding junction.

In the weak coupling limit and for a short superconducting region no zero bias peak appears in the conductance spectrum (figure 6.12(a)), while if we increase the length of the superconducting region the peak appears again (figure 6.12(b)).

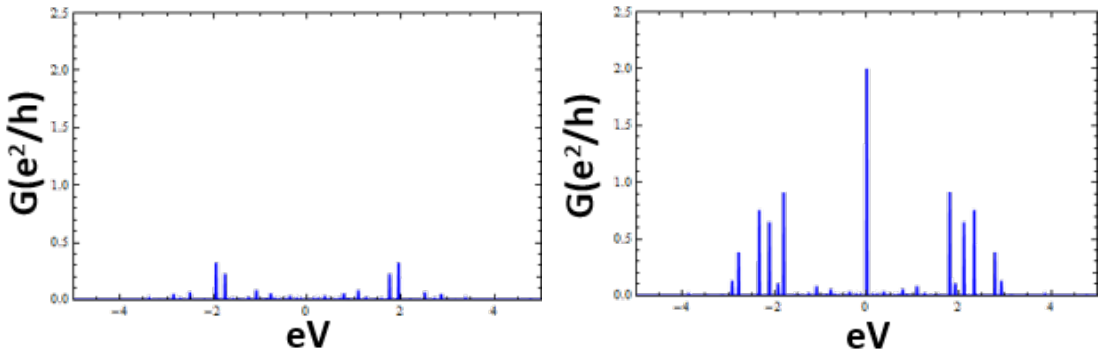

(a) *(b)*

Figure 6.12: (a) Conductance for a phase-winding junction where a sudden variation of the superconducting phase occurs and the leads are weakly coupled to the chain. (b) Conductance for a phase-winding junction where the superconducting phase varies gradually and the leads are weakly coupled (tlead = tchain = 4.0 and tcouple = 0.2).

Thus we confirm that, when the superconducting phase suddenly changes from 0 to π, the phase-winding junction behaves similarly to the real π-junction. Moreover, also in this case the length of the superconducting region has to be sufficiently "small" and the junction should be placed on the center of the superconducting region in order for the resonant transmission at the T_{ee} channel to take place.

The exact profiles of the superconducting order parameter for all the setups that were discussed in this chapter are given in Appendix C.

Chapter 7

Summary and discussion

In this work we reviewed the one-dimensional spinless p-wave superconductor that was introduced by Kitaev. We also discussed the link between topology and condensed matter physics and focused on the different topological phases that arise in this model by examining the properties of the real π-junction and of the phase winding junction.

Next, we considered a tri-junction setup, where the ends of three Kitaev wires are brought close together and the three Majorana zero modes at the ends interact with each other. We numerically simulated this configuration and took advantage of the properties of the π-junctions in order to explain the interaction between the zero modes. We saw that in this setup, due to the nature of the p-wave pairing, one cannot avoid the formation of a π-junction between at least two of the wires. Because the Majorana modes can only gap out in pairs, the number of such modes in the junction is always odd.

In chapter 5, we reviewed the Green's function formalism for describing the transport properties of superconducting systems and employed the Landauer-Büttiker formula to obtain the expression for the conductance of the NS and of the NSN junctions. Using this approach we developed a numerical implementation in order to simulate the transport properties of these junctions. For the NS junction, when the lead is weakly coupled to the Kitaev chain, we verified the existence of the zero bias peak in the conductance spectrum that is alleged to be a characteristic signature of the Majorana zero mode.

Concerning the conductance measurements of the NSN junction, we found that when the superconducting order parameter takes a constant value along the Kitaev chain the only process that contributes to the subgap conductance is the local Andreev reflection. When the leads are perfectly coupled to the chain the transmission probability for this process, in the subgap region, is equal to 1 and the conductance is equal to $2\frac{e^2}{h}$. On the other hand, when the coupling between the leads and the chain becomes weaker the local Andreev reflection probability is suppressed everywhere except at zero bias. The presence of the zero bias peak in the weak coupling limit is alleged to be a characteristic signature of a Majorana zero mode. This peak does not depend on the length of the superconducting region since it is created by a strictly local process (i.e. not a tunneling through a finite barrier).

By exploiting the properties of the real π-junction and of the phase winding junction we learned that things change when a fermionic zero mode is localized at the center of the junction. When the leads are perfectly coupled to the chain, and the superconducting region is sufficiently small, a dip is observed at zero bias in the conductance spectrum. It turns out that the resonant transmission of an electron through the chain is responsible for this dip and this results in the suppression of the local Andreev process at zero bias. Thus when we weaken the coupling between the leads and the chain no peak survives in the conductance. On the contrary when the length of the superconducting region is increased and the leads are perfectly coupled, only the local Andreev process contributes to the conductance and the dip disappears. As a result when the coupling is decreased the zero bias peak in the conductance persists.

The tunneling of an electron through the Kitaev chain is a process that strictly depends on that a fermionic mode sits exactly at zero energy at the center of the superconducting region. Thus it seems that the existence of the condensate affects this process and that one could describe

it in the following way. Imagine that the fermionic mode at the center of the junction is occupied and an electron enter inside the superconductor from the left, these two electrons can now form a Cooper pair. Afterwards the opposite happens, the Cooper pair desolves, the mode at the center is reoccupied and an electron pops out at the right side. For this process to occur, the length of the superconducting region from the left side of the junction should be equal to the one on the right otherwise no resonant transmission can be achieved, this is in agreement with what we have observed in our numerical simulations.

However we saw that when we exceed a maximum length of the superconducting region the resonant is suppressed, this does not fit with our explanation since the only important length scale should be the coherence length of the superconductor and for the particular profiles that we have chosen in our simulations this length scale is just a few sites and does not seem to play an important role. So the exact mechanism responsible for the appearance of the zero bias dip in the conductance spectrum remains an interesting open question.

Bibliography

[1] Jason Alicea. New directions in the pursuit of majorana fermions in solid state systems. *Reports on Progress in Physics*, 75(7):076501, 2012.

[2] Jason Alicea, Yuval Oreg, Gil Refael, Felix von Oppen, and Matthew PA Fisher. Non-abelian statistics and topological quantum information processing in 1d wire networks. *Nature Physics*, 7(5):412–417, 2011.

[3] Alexander Altland and Ben D Simons. *Condensed matter field theory*. Cambridge University Press, 2010.

[4] Alexander Altland and Martin R Zirnbauer. Nonstandard symmetry classes in mesoscopic normal-superconducting hybrid structures. *Physical Review B*, 55(2):1142, 1997.

[5] GE Blonder, M Tinkham, and TM Klapwijk. Transition from metallic to tunneling regimes in superconducting microconstrictions: Excess current, charge imbalance, and supercurrent conversion. *Physical Review B*, 25(7):4515, 1982.

[6] M Buttiker. Four-terminal phase-coherent conductance. *Physical Review Letters*, 57(14):1761, 1986.

[7] Supriyo Datta. *Electronic transport in mesoscopic systems*. Cambridge university press, 1997.

[8] Supriyo Datta. Nanoscale device modeling: the greens function method. *Superlattices and microstructures*, 28(4):253–278, 2000.

[9] Supriyo Datta, Philip F Bagwell, and MP Anantram. Scattering theory of transport for mesoscopic superconductors. 1996.

[10] Steven R Elliott and Marcel Franz. Colloquium: Majorana fermions in nuclear, particle, and solid-state physics. *Reviews of Modern Physics*, 87(1):137, 2015.

[11] Marcel Franz. Majorana's wires. *Nature nanotechnology*, 8(3):149–152, 2013.

[12] Sven Gnutzmann and Uzy Smilansky. Quantum graphs: Applications to quantum chaos and universal spectral statistics. *Advances in Physics*, 55(5-6):527–625, 2006.

[13] K Ishida, H Mukuda, Y Kitaoka, K Asayama, ZQ Mao, Y Mori, and Y Maeno. Spin-triplet superconductivity in sr2ruo4 identified by 17o knight shift. *Nature*, 396(6712):658–660, 1998.

[14] Thomas WB Kibble. Topology of cosmic domains and strings. *Journal of Physics A: Mathematical and General*, 9(8):1387, 1976.

[15] A Yu Kitaev. Unpaired majorana fermions in quantum wires. *Physics-Uspekhi*, 44(10S):131, 2001.

[16] Alexei Kitaev. Periodic table for topological insulators and superconductors. *arXiv preprint arXiv:0901.2686*, 2009.

[17] HV Klapdor-Kleingrothaus, A Dietz, HL Harney, and IV Krivosheina. Evidence for neutrinoless double beta decay. *Modern Physics Letters A*, 16(37):2409–2420, 2001.

[18] NB Kopnin and MM Salomaa. Mutual friction in superfluid he 3: Effects of bound states in the vortex core. *Physical Review B*, 44(17):9667, 1991.

[19] Rolf Landauer. Electrical resistance of disordered one-dimensional lattices. *Philosophical Magazine*, 21(172):863–867, 1970.

[20] Jie Liu, Andrew C Potter, KT Law, and Patrick A Lee. Zero-bias peaks in the tunneling conductance of spin-orbit-coupled superconducting wires with and without majorana end-states. *Physical review letters*, 109(26):267002, 2012.

[21] Ettore Majorana. Teoria simmetrica dellelettrone e del positrone. *Il Nuovo Cimento*, 14(4):171–184, 1937.

[22] Vincent Mourik, Kun Zuo, SM Frolov, SR Plissard, EPAM Bakkers, and LP Kouwenhoven. Signatures of majorana fermions in hybrid superconductor-semiconductor nanowire devices. *Science*, 336(6084):1003–1007, 2012.

[23] Stevan Nadj-Perge, Ilya K Drozdov, Jian Li, Hua Chen, Sangjun Jeon, Jungpil Seo, Allan H MacDonald, B Andrei Bernevig, and Ali Yazdani. Observation of majorana fermions in ferromagnetic atomic chains on a superconductor. *Science*, 346(6209):602–607, 2014.

[24] Yuval Oreg, Gil Refael, and Felix von Oppen. Helical liquids and majorana bound states in quantum wires. *Physical review letters*, 105(17):177002, 2010.

[25] Nicholas Read and Dmitry Green. Paired states of fermions in two dimensions with breaking of parity and time-reversal symmetries and the fractional quantum hall effect. *Physical Review B*, 61(15):10267, 2000.

[26] Dmitry A Ryndyk. Theory of quantum transport at nanoscale.

[27] Jay D Sau, Roman M Lutchyn, Sumanta Tewari, and S Das Sarma. Generic new platform for topological quantum computation using semiconductor heterostructures. *Physical review letters*, 104(4):040502, 2010.

[28] Andreas P Schnyder, Shinsei Ryu, Akira Furusaki, and Andreas WW Ludwig. Classification of topological insulators and superconductors in three spatial dimensions. *Physical Review B*, 78(19):195125, 2008.

[29] C. Spånslätt, E. Ardonne, J. C. Budich, and T. H. Hansson. Topological aspects of π phase winding junctions in superconducting wires. *arXiv preprint arXiv:1501.03413v2*, 2015.

[30] Daniel C Tsui, Horst L Stormer, and Arthur C Gossard. Two-dimensional magnetotransport in the extreme quantum limit. *Physical Review Letters*, 48(22):1559, 1982.

[31] Steven Weinberg. *The quantum theory of fields*, volume 1. Cambridge university press, 1995.

[32] Xiao-Gang Wen. Vacuum degeneracy of chiral spin states in compactified space. *Physical Review B*, 40(10):7387, 1989.

[33] Xiao-Gang Wen, Yong-Shi Wu, and Yasuhiro Hatsugai. Chiral operator product algebra and edge excitations of a fractional quantum hall droplet. *Nuclear Physics B*, 422(3):476–494, 1994.

[34] Frank Wilczek. Majorana returns. *Nature Physics*, 5(9):614–618, 2009.

Appendix A

Derivation of the conductance formula

Here we will derive the conductance formula for the NSN junction, we will assume that two normal wires are connected at the two ends of a superconducting chain and a voltage difference eV is applied between them. We are free to choose the voltage on the right lead to be equal to zero. Moreover we will assume that all the chemichal potentials and the temperature are equal to zero. By using the Landauer-Buttiker formula we can write the formula for the current in the left electron lead:

$$\begin{aligned} I_{e1} =& \frac{e}{h}\int_0^\infty dE\Big[\Big(f_{e2}-f_{e1}\Big)T_{e1,e2}+(f_{h2}-f_{e1}\Big)T_{e1,h2}+\Big((f_{h1}-f_{e1}\Big)T_{e1,h1}\Big] \\ =& \frac{e}{h}\int_0^\infty dE\Big(T_{e1,e2}f_{e2}-T_{e1,e2}f_{e1}+T_{e1,h2}f_{h2}-T_{e1,h2}f_{e1}+T_{e1,h1}f_{h1}-T_{e1,h1}f_{e1}\Big) \end{aligned} \tag{A.1}$$

The terms which are colored are functions of the applied voltage, for our discussion all the other terms can be neglected since they will eventually "die" when we will take the derivative with respect to the voltage in order to obtain the conductance. Using the flux conservation $T_{e1,e2}+T_{e1,h1}+T_{e1,e1}+T_{e1,h2}=1$ and keeping only the terms that are functions of the voltage we can write the above relation as:

$$I_{e1} = -\frac{e}{h}\int_0^\infty dE\Big[(1-T_{e1,e1})f_{e1}-T_{e1,h1}f_{h1}\Big] \tag{A.2}$$

At zero temperature the Fermi distribution becomes a Θ-function. The first term of equation A.2 becomes:

$$1st-term = -\frac{e}{h}\int_0^\infty dE\Big(1-T_{e1,e1}\Big)\Theta(-E+\mu_0+eV) \tag{A.3}$$

while the second term:

$$\begin{aligned} 2nd-term =& \frac{e}{h}\int_0^\infty dE \quad T_{e1,h1}f_{h1} = \frac{e}{h}\int_{-\infty}^0 dE \quad T_{e1,h1}(-E)f_{h1}(-E) \\ =& \frac{e}{h}\int_{-\infty}^0 dE \quad T_{h1,e1}(E)\Big(1-f_{e1}(E)\Big) \end{aligned} \tag{A.4}$$

where we have set $E\to -E$ and used the fact that due to particle-hole symmetry $f_{h1}(-E)=1-f_{e1}(E)$ and $T_{ij}(-E)=T_{ji}(E)$. Again by keeping only the voltage dependent term we can write:

$$2nd-term = -\frac{e}{h}\int_{-\infty}^0 dE \quad T_{h1,e1}\Theta(-E+\mu_0+eV) \tag{A.5}$$

By looking at equation A.2 we can imediately write down the formula for the current in the left hole lead:

$$I_{h1} = \frac{e}{h}\int_0^\infty dE\Big[(1-T_{h1,h1})f_{h1}-T_{h1,e1}f_{e1}\Big] \tag{A.6}$$

Using the same arguments we have used for the electron current, the two terms of equation A.6 become:

$$1st - term = -\frac{e}{h}\int_{-\infty}^{0} dE\Big(1 - T_{e1,e1}\Big)\Theta(-E + \mu_0 + eV) \tag{A.7}$$

$$2nd - term = -\frac{e}{h}\int_{0}^{\infty} dE \quad T_{h1,e1}\Theta(-E + \mu_0 + eV) \tag{A.8}$$

The total current will be $I_1 = I_{e1} + I_{h1}$, thus by combining all the above we obtain:

$$I_1 = -\frac{e}{h}\int_{-\infty}^{\infty} dE\Big[1 - T_{e1,e1} + T_{h2,e2}\Big]\Theta(-E + \mu_0 + eV) \tag{A.9}$$

Finally, knowing that $\mu_0 = 0$ and taking the derivative with respect to the voltage the conductance formula is derived.

$$\mathcal{G}_{NSN} = \frac{\partial I_1}{\partial V} = -\frac{e^2}{h}\Big[1 - T_{e1,e1}(eV) + T_{h1,e1}(eV)\Big] \tag{A.10}$$

Appendix B

Coupling between two wires

Let us assume that we have two topological wires, where the last site of the first wire is connected to the first site of the second wire, with a real hopping amplitude t_{12} and a superconducting coupling $\Delta_{12}e^{i\phi_{12}}$. The Hamiltonian which connects these two sites is:

$$\mathcal{H}_c = -\frac{t_{12}}{2}(c_1^\dagger c_2 + c_2^\dagger c_1) - \frac{|\Delta_{12}|}{2}(e^{i\phi_{12}}c_1 c_2 + e^{-i\phi_{12}}c_2^\dagger c_1^\dagger) \tag{B.1}$$

where by c_1 we denote the last site of the first wire and by c_2 the first site of the second wire. Furthermore, we will assume that in each wire $\Delta = t$ and $\mu = 0$, so that the Majorana zero modes are perfectly localized at the two ends of the wires. By using the trasformations:

$$c_n = \frac{ie^{-i\frac{\phi}{2}}\gamma_{2n-1} - e^{-i\frac{\phi}{2}}\gamma_{2n}}{2i}, \qquad c_n^\dagger = \frac{e^{i\frac{\phi}{2}}\gamma_{2n} + ie^{i\frac{\phi}{2}}\gamma_{2n-1}}{2i} \tag{B.2}$$

we can replace the fermionic operators with the Majorana operators and the Hamiltonian becomes:

$$\begin{aligned}
\mathcal{H}_c = &-\frac{t_{12}}{2}\Big[\frac{1}{4}e^{i\phi_1/2}(\gamma_{B,1} - i\gamma_{A,1})e^{-i\phi_2/2}(\gamma_{B,2} + i\gamma_{A,2})\Big] \\
&-\frac{t_{12}}{2}\Big[\frac{1}{4}e^{i\phi_2/2}(\gamma_{B,2} - i\gamma_{A,2})e^{-i\phi_1/2}(\gamma_{B,1} + i\gamma_{A,1})\Big] \\
&+\frac{|\Delta_{12}|}{2}e^{i\phi_{12}}\Big[\frac{1}{4}e^{-i\phi_1/2}(\gamma_{B,1} + i\gamma_{A,1})e^{-i\phi_2/2}(\gamma_{B,2} + i\gamma_{A,2})\Big] \\
&+\frac{|\Delta_{12}|}{2}e^{-i\phi_{12}}\Big[\frac{1}{4}e^{i\phi_2/2}(\gamma_{B,2} - i\gamma_{A,2})e^{i\phi_1/2}(\gamma_{B,1} - i\gamma_{A,1})\Big]
\end{aligned} \tag{B.3}$$

Since we are interested in explaining how the two Majorana modes interact with each other we will only keep the corresponding terms:

$$\begin{aligned}
\mathcal{H}_c = &-\frac{t_{12}}{8}\Big(i\gamma_{B,1}\gamma_{A,2}e^{i(\phi_1-\phi_2)/2} - i\gamma_{A,2}\gamma_{B,1}e^{i(\phi_2-\phi_1)/2}\Big) \\
&-\frac{|\Delta_{12}|}{8}\Big(i\gamma_{B,1}\gamma_{A,2}e^{i\phi_{12}-i(\phi_1+\phi_2)/2} - i\gamma_{A,2}\gamma_{B,1}e^{i\phi_{12}+i(\phi_2+\phi_1)/2}\Big)
\end{aligned} \tag{B.4}$$

By using the fermionic commutation relations and get rid of one of the indices we arrive at:

$$\mathcal{H}_{\gamma\gamma} = -i\frac{t_{12}}{4}\cos\Big(\frac{\phi_1 - \phi_2}{2}\Big)\gamma_1\gamma_2 - i\frac{|\Delta_{12}|}{4}\cos\Big(\phi_{12} - \frac{\phi_1 + \phi_2}{2}\Big)\gamma_1\gamma_2 \tag{B.5}$$

Appendix C

Profiles for the superconducting order parameter

Here we present the different profiles that were used in chapter 6, for the three cases that were studied.

C.1 Constant superconducting order parameter

The profile for the order parameter that was used in this case is depicted in the following plot, the superconducting order parameter is exponentially increased up to a constant value and then falls down in the exact same way at the other end of the superconducting region.

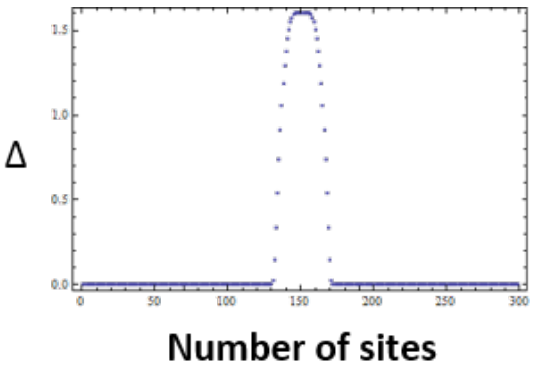

Figure C.1: Profile for the superconducting order parameter.

C.2 Real pi-junction

To form a real π junction we used the profile for the superconducting order parameter that is depicted in figure C.2 and in order to investigate what happens when the length of the superconducting region is increased we add sites of constant Δ ($\Delta = 1.5$ and $\Delta = -1.5$) in this profile.

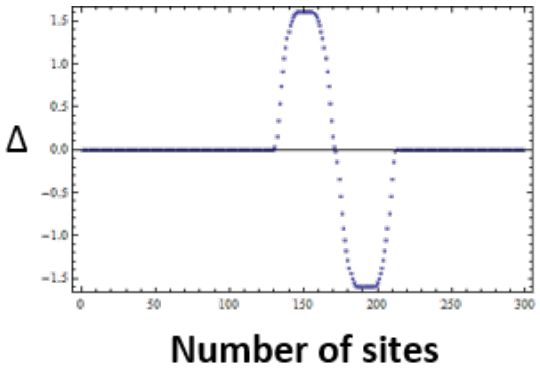

Figure C.2: Profile for the superconducting order parameter.

C.3 Phase winding junction

In the case of the phase-winding junction the absolute value of the order parameter remains constant and the only thing that changes is the superconducting phase. Figures C.4 and C.5 illustrate the exact phase profiles that we used for our numerical simulations.

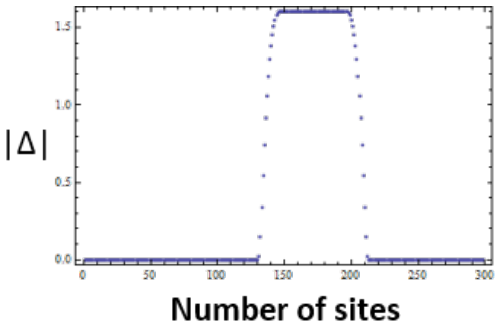

Figure C.3: Profile for the absolute value of the superconducting order parameter.

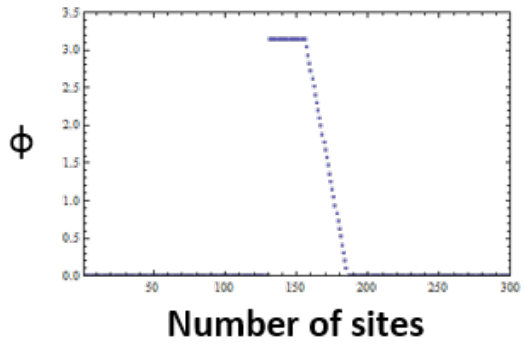

Figure C.4: Profile for the superconducting phase. The variation of the phase from 0 *to* π *occurs linearly over* 30 *sites.*

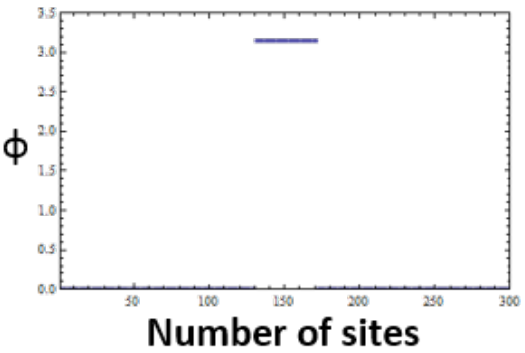

Figure C.5: Profile for the superconducting phase. The width of the junction in this case is "zero" (the variation takes place over one site).